4-1993

Non-Resonant Transfer and Excitation for S^13+ Projectiles Colliding with Neutral Gas Targets

Liang Duo
Western Michigan University

NON-RESONANT TRANSFER AND EXCITATION FOR S^{13+} PROJECTILES COLLIDING WITH NEUTRAL GAS TARGETS

by

Liang Duo

A Thesis
Submitted to the
Faculty of The Graduate College
in partial fulfillment of the
requirements for the
Degree of Master of Arts
Department of Physics

Western Michigan University
Kalamazoo, Michigan
April 1993

NON-RESONANT TRANSFER AND EXCITATION FOR S^{13+} PROJECTILES COLLIDING WITH NEUTRAL GAS TARGETS

Liang Duo, M.A.

Western Michigan University, 1993

Non-resonant Transfer and Excitation (NTE) by 20-70 Mev S^{13+} projectiles in collisions with neutral gas targets of He, Ne and Ar is investigated. For NTE, positively charged projectiles undergo excitation and electron capture in a single collision in which the capture and excitation processes are independent events. The mechanisms involved in the NTE process are electron-nucleus interactions, and the combination of projectile excitation and capture is a two-step process. In this work, NTE cross sections, along with total K x-ray production cross sections and total single-electron capture and loss cross sections, were measured as a function of projectile energy. The results are used to establish the dependence of NTE on the atomic number of the target. The present results for S^{13+} incident on He are consistent with the results of Tanis et al. (1985) which indicate that a maximum in the NTE cross section occurs at about 30 MeV. It is found here that for Ne and Ar the maximum NTE cross section occurs at about 50 MeV and 60 MeV, respectively. Thus, with increasing target atomic number, NTE occurs for higher projectile energies.

ACKNOWLEDGMETS

I wish to express my sincere gratitude and appreciation to my advisor, Professor John A. Tanis, for his patience, guidance and assistance in the completion of this research project. My thanks are extended also to Dr. Roger Haar for his help and cooperation in preparing and perform ing the experimental work conducted for this thesis, and to Dr. Steve Ferguson for operating the accelerator throughout this research.

I would like to thank Dr. Robert Shamu and Dr. Roger Haar for their suggestions and comments as the members of my committee.

My special thanks are for my wife, Ying-li Luan, for her love, support and encouragement. My daughter, Joy Duo, has given me happy and pleasant times.

Liang Duo

Order Number 1352177

Non-resonant transfer and excitation for S^{13+} projectiles colliding with neutral gas targets

Duo, Liang, M.A.

Western Michigan University, 1993

U·M·I
300 N. Zeeb Rd.
Ann Arbor, MI 48106

TABLE OF CONTENTS

LIST OF TABLES

LIST OF FIGURES

List of Figures--Continued

CHAPTER I

INTRODUCTION

In considering collisions between positively charged projectile ions and neutral target atoms, three mechanisms are important, namely, excitation, ionization, and charge transfer. In the excitation process, one or more electrons are excited from lower to higher energy states within the projectile ion or the target atom, and vacancies are produced in the energy levels originally occupied by the excited electrons. The decay of the resulting intermediate excited state, in which an electron "falls" from a higher to a lower energy level, can be detected by x-ray emission or Auger electron emission. In the ionization process, one or more electrons are lost from the projectile ion or the neutral target atom. In charge transfer, electrons from one collision partner are transferred (or captured) to the other collision partner.

Generally speaking, all three processes are related since they can be attributed to the Coulomb force between the projectile ions and the target atoms, specifically, the direct Coulomb interaction between the nucleus of one colliding partner and the electrons of the other, or

between the projectile electrons and target electrons. The basic parameters governing the three major categories of events are the distance between the particles (impact parameter), the charge state, and the projectile energy.

In addition to the individual processes, combinations of excitation, ionization, and electron transfer can occur in a single collision between a projectile ion and a target atom. The primary emphasis of this thesis is the study of combined electron capture and projectile excitation in a single ion-atom collision. The intermediate excited state which is formed can decay by either Auger electron emission or photon emission. Which of these decay modes predominates depends on the intermediate state of the ion and its atomic number. In this work, the observation of x-ray emission, resulting from decay of the intermediate excited state, associated with electron capture is used to identify the combined collision process.

When projectile excitation and charge transfer occur together in a single collision, it is important to note that the capture and excitation can be either a correlated or an uncorrelated process, since there are two mechanisms by which this combined electron transfer and ion excitation can proceed. The correlated process is called resonant-transfer and excitation (RTE) (Tanis et al., 1982), while the uncorrelated two-step process is called non-resonant-transfer and excitation (NTE) (Pepmiller et al., 1983 and

1985).

For RTE, the combined process of electron transfer and projectile excitation takes place simultaneously. The mechanism involved is an electron-electron interaction between a projectile electron and a weakly bound target electron. RTE is similar to the inverse of an Auger transition, which means that the projectile ion passes through exactly the same states as in the Auger process but in reverse order. Resonant formation of the intermediate excited states occurs for incident projectile ion energies such that the target electron energy, in the rest frame of the ion, equals one of the Auger electron energies. RTE is analogous to the mechanism called dielectronic recombination (DR) except that for DR the captured electron is initially free instead of bound (Tanis, 1987).

In the NTE process, the combination of electron capture and projectile excitation is a two-step process which does not depend resonantly on the incident projectile energy. The mechanisms involved in the NTE process are electron-nucleus interactions. The interaction between the projectile nucleus and a target electron results in electron capture, while the interaction between the target nucleus and a projectile electron results in projectile excitation. For NTE, electron capture and projectile excitation are independent processes. Experiments designed to investigate NTE are essentially the same as those

designed to study RTE but require lower projectile energies, since NTE occurs at lower projectile energies in comparison with RTE (Tanis et al., 1985).

It is the purpose of this thesis to study NTE using Li-like sulfur S^{13+} as projectiles incident on several neutral gas targets, namely, He, Ne and Ar, to obtain the target atomic number dependence of NTE. In addition to NTE, combined electron loss and projectile K excitation, total projectile K x-ray emission, and total single-electron capture and loss have been investigated. Also, projectile electron capture and loss associated with target K x-ray emission were measured but will not be considered here.

The measurements conducted here to investigate NTE utilized coincidence techniques. The combined process of electron capture and projectile excitation in single collisions has been identified and investigated by measuring the energy dependence of the yield of deexcitation photons coincident with projectiles which have captured an electron. Experimentally, NTE and RTE have the same signature, but the mechanisms leading to NTE and RTE are very different. To date, only a few NTE experiments have been reported (Pepmiller et al., 1985, and Tanis et al., 1985 and 1986). The focus of this work is to try to more fully understand the NTE process.

In the next chapter, the theoretical description of RTE and NTE is outlined. The experiment for NTE, in which the author was a participant, will be discussed in detail in Chapter III, and the data analysis techniques, especially the calculation of the experimental cross sections of interest and the experimental results, are presented in tables as well as displayed in graphs in Chapter IV. In Chapter V, a discussion of the experimental results is given, which also contains a comparison of previous results to the present experimental results. Finally, the conclusions resulting from this work are summarized in Chapter VI.

CHAPTER II

THEORETICAL DESCRIPTIONS

In the collision between a projectile ion and a target atom, the Coulomb interaction between the colliding particles leads to electronic rearrangement by means of excitation, ionization, and charge transfer. In general, if both collision partners initially carry electrons, the electron-electron interaction and the electron-nucleus interaction must be considered in these processes.

As noted in Chapter I, in an ion-atom collision, projectile excitation and electron capture from the target atom can occur together in a single encounter resulting in the formation of an intermediate doubly-excited state. The intermediate excited state decays by either photon (x-ray) emission or electron (Auger) emission, and the entire reaction is described by the following equation

$$A^{q+} + B \longrightarrow [\ A^{(q-1)+}\ ]^{**} + B^{+} \qquad (2.1a)$$

$$\longrightarrow A^{(q-1)+} + h\nu \qquad (2.1b)$$

$$\longrightarrow A^{q+} + e^{-}. \qquad (2.1c)$$

This combined electron capture and excitation process can be correlated (RTE) or uncorrelated (NTE). Each of these processes will be considered separately here.

RTE

RTE is one-step process, and the mechanism involved is an electron-electron interaction between a projectile electron and a (weakly-bound) target electron, similar to the inverse of an Auger transition as shown in Figure 1. RTE is very similar to dielectronic recombination (DR) except that DR involves the interaction between an ion and a free electron. In RTE, simultaneous electron capture and projectile excitation occurs only when the relative velocity between the projectile ion and the incoming electron equals the velocity of an ejected Auger electron. An energy-level schematic of the RTE process for a Li-like ion is shown in Figure 2.

In a formal theoretical treatment of RTE, Brandt (1983a) proposed that RTE could be formulated in the impulse approximation, which states that immediately after the collision the separation between the projectile and target is such that there is no further interaction. The impulse approximation requires that the incident ion velocity be much greater than the velocity of the captured electron (i.e., $V_{ion} >> V_{electron}$), thereby approximating a

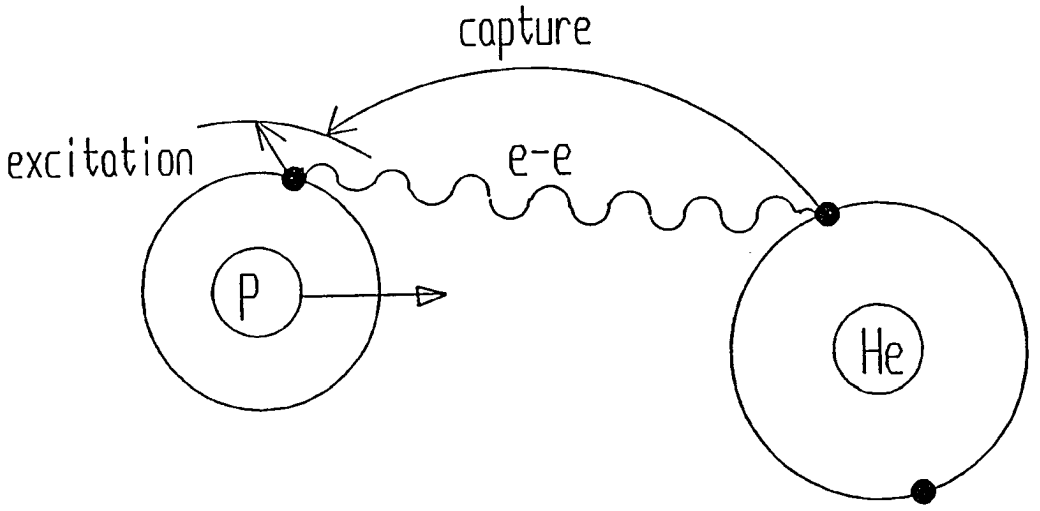

Figure 1. Schematic Diagram Indicating How the Electron-Electron Interaction Leads to Simultaneous Electron Capture and Projectile Excitation in the RTE Process.

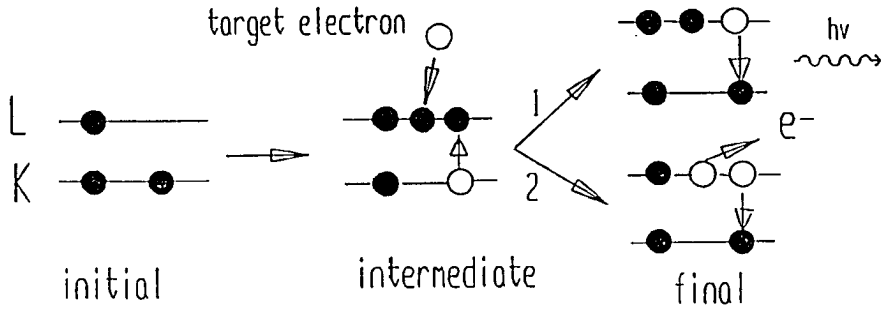

$$S^{13+} + He \rightarrow (S^{12+})^{**} + He^{+} \quad \begin{matrix} 1 \rightarrow S^{12+} + h\nu + He^{+} \\ 2 \rightarrow S^{13+} + e^{-} + He^{+} \end{matrix}$$

Figure 2. Energy-level Schematic of the RTE Process for a Li-like Ion.

Simultaneous electron capture and projectile excitation result in the formation of an intermediate doubly-excited state. The intermediate excited state subsequently decays by either photon emission (1) or electron emission (2).

collision between an ion and a free electron. It is concluded that, in first order, RTE is equivalent to dielectronic recombination averaged over the electron momentum distribution of the target electrons. Then, the RTE cross section can be expressed by

$$\sigma_{RTE} \sim \sigma_{DR} \sum J_i(P_{iz}) \qquad (2.2)$$

where σ_{RTE} is the RTE cross section, σ_{DR} is the DR cross section, and $J_i(P_{iz})$ is the Compton profile (momentum distribution) of the target electrons, which is the probability of finding a particular target electron with momentum component P_{iz} along the beam axis. In general, the calculation of DR cross sections is difficult, but results for several ions have been reported to date (Hahn & LaGattuta, 1988).

NTE

The process of principal interest here is non resonant transfer and excitation (NTE), which is a two-step process giving rise to the same intermediate excited states as RTE (or DR). Though the NTE mechanism, which is uncorrelated since it involves two separate electron-nucleus interactions as shown in Figure 3, is unrelated to the single-step RTE mechanism, the resulting doubly-excited intermedi-

ate states and their subsequent decay by photon (x-ray) emission are experimentally indistinguishable from those formed in the RTE process. Since NTE and RTE both can produce the same intermediate excited states and can decay in same way, as indicated in Figure 4, NTE is considered a competing process. However, the theoretical treatment (Brandt, 1983a,b) and experimental results (J.A. Tanis, 1987) indicated that NTE is generally expected to be dominant at projectile energies lower than those for which RTE occurs. Thus, in order to investigate the NTE process in ion-atom collisions, measurements must be conducted at lower projectile energies.

For NTE, the electron capture and excitation events are independent, i.e., no resonant conditions are involved. The formation of the intermediate excited state occurs by excitation of a projectile electron through the Coulomb interaction with the target nucleus, and, in the same encounter, the projectile ion captures an electron from the target. Figure 3 illustrates schematically the NTE mechanism involving these two separate electron-nucleus interactions. The general shapes of the K-shell excitation cross section and the capture probability to the L (or higher) shell for highly charged projectile ions incident on neutral target atoms are illustrated in Figure 5. For the electron capture process, the cross section is large at

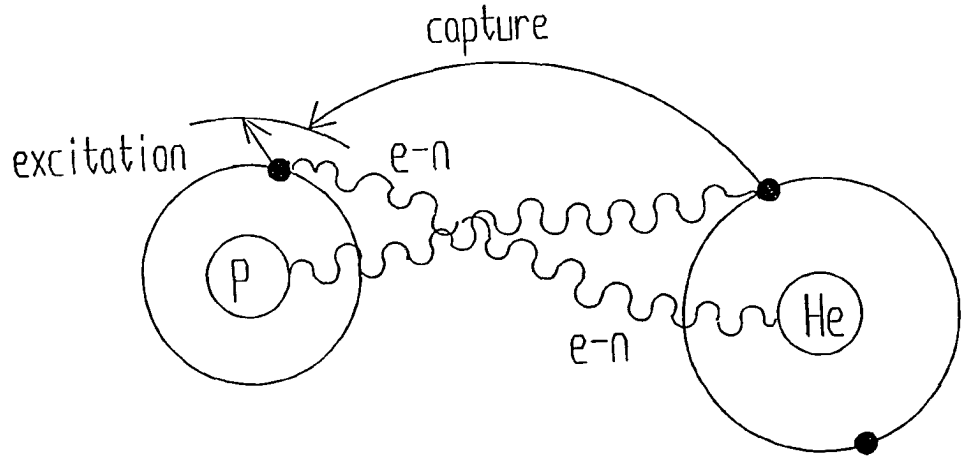

Figure 3. Schematic Indicating How Electron-Nucleus Interactions Lead to NTE.

The interaction between the projectile nucleus and a target electron results in electron capture, and the interaction between the target nucleus and a projectile electron results in projectile excitation.

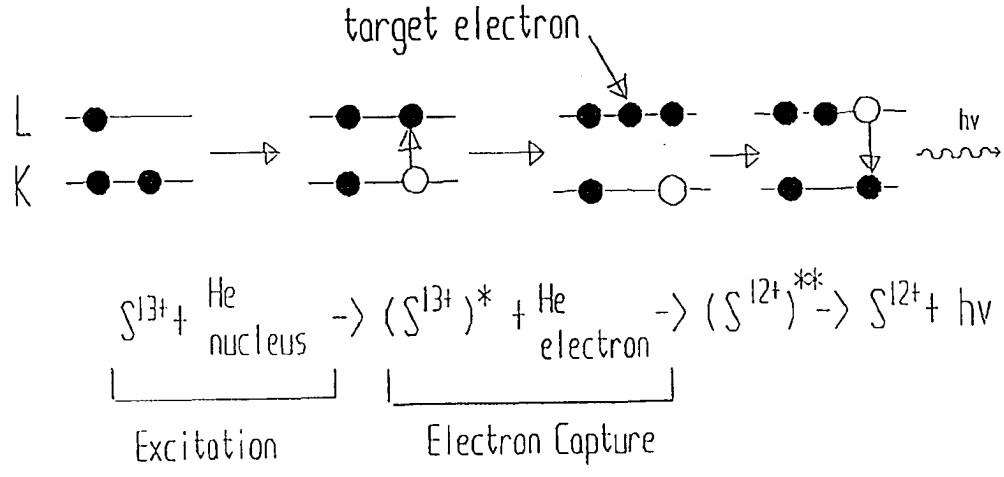

Figure 4. Energy-Level Schematic of a Possible NTE Process for a Li-Like Ion.

Independent electron capture and projectile excitation events result in the formation of a doubly-excited intermediate state.

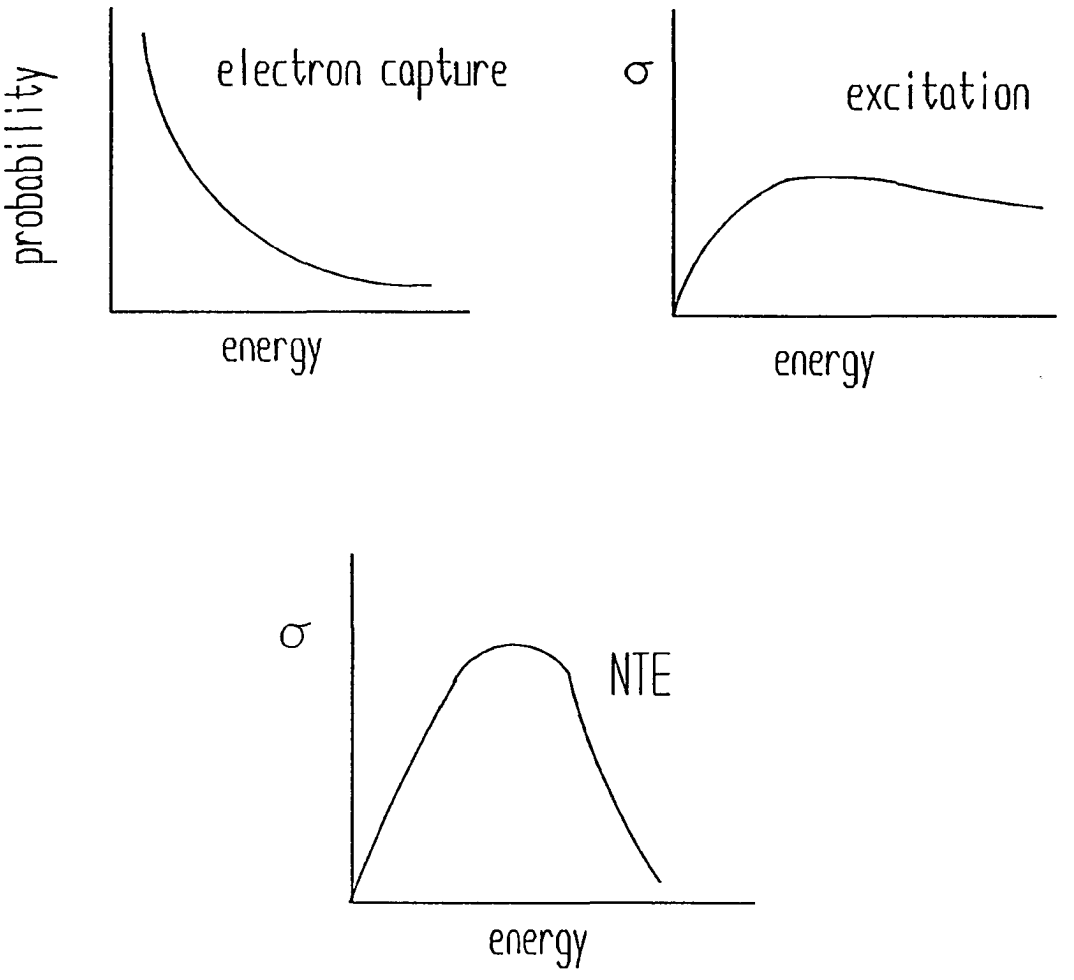

Figure 5. Qualitative Representation of the L-shell Capture Probability, P_{cap} the K-shell Excitation Cross Section σ_{ex}, and the Resulting NTE Cross Section σ_{NTE} Which is a Product of the Capture Probability and the Excitation Cross Section.

low projectile energies and decreases exponentially as the energy is increased. For excitation events, the cross section increases rapidly at low energies, reaches a maximum, and then decreases slowly at higher energies.

Since NTE is a two-step process in which electron capture and projectile excitation are independent, the cross section for NTE is proportional to the product of the probabilities for capture and excitation (Pepmiller et al., 1983 and 1985). The probabilities for capture and excitation are functions of the impact parameter b, so the NTE cross section can be expressed by the following:

$$\sigma_{NTE} = 2\pi \int_0^\infty P_{cap}(b) \cdot P_{ex}(b) \cdot b\,db \qquad (2.3)$$

where the integral is over all impact parameters. $P_{cap}(b)$ is the probability for the captured target electron to go to the L (or higher) shell of the ion, and $P_{ex}(b)$ is the probability for K-shell excitation of the ion. Over the range of b where $P_{ex}(b)$ is nonzero, the capture probability $P_{cap}(b)$ is approximately constant and equal to $P_{cap}(0)$, i.e., the capture probability at zero impact parameter. For $P_{cap}(b) \approx P_{cap}(0) =$ constant, it can be taken out of the integral, so that

$$\sigma_{NTE} \approx P_{cap}(0)\, 2\pi \int_0^\infty P_{ex}(b) \cdot b\,db \qquad (2.4)$$

Thus, the NTE cross section can be expressed as

$$\sigma_{NTE} \approx P_{cap}(0) \cdot \sigma_{ex} \qquad (2.5)$$

where the cross section for projectile excitation is given by

$$\sigma_{ex} = 2\pi \int_0^\infty P_{ex}(b) \cdot b\,db \ . \qquad (2.6)$$

Since for NTE, as discussed above, the capture and excitation processes are independent, the qualitative shape of the NTE cross section can be obtained by multiplying σ_{ex} and P_{cap}.

The magnitude of the NTE cross section depends on the projectile energy, the charge state and atomic number of projectile, and the atomic number of the target. In collisions of an ion with targets of increasingly higher atomic number Z, the Coulomb interaction between the target nucleus and the projectile electron, which gives rise to projectile excitation, becomes stronger, so that the probability for projectile excitation gets larger. Also, since the number of electrons in the target increases with Z, the capture probability is increased. It can be expected that, by investigating NTE for the same projectile ion but different target atoms, the magnitude of the NTE cross section will become larger for targets with

higher atomic numbers.

CHAPTER III

EXPERIMENTAL PROCEDURE

Non resonant transfer and excitation (NTE) was investigated for Li-like S^{13+} projectiles incidient on He, Ne, and Ar target gases. The experiments were performed using the 6-MV tandem Van de Graaff accelerator at Western Michigan University. A general schematic of the accelerator facility is shown in Figure 6.

First, negative sulfur ions were produced by a SNICS ion source (i.e., Source of Negative Ions by Cesium Sputtering). These sources are one of the most widely used negative ion sources in tandem accelerator laboratories. The negative ions extracted from the source are accelerated toward the positive high-voltage terminal of the accelerator. At the terminal, the negative ions are passed through a carbon stripping foil causing electrons to be removed. The resulting positive sulfur ions are then accelerated away from the terminal. To reach the highest beam energy (70MeV), a second stripping foil, located between the positive terminal and the high-energy end of the accelerator, was used to produced even higher charge states thereby giving rise to additional acceleration. Ions of the

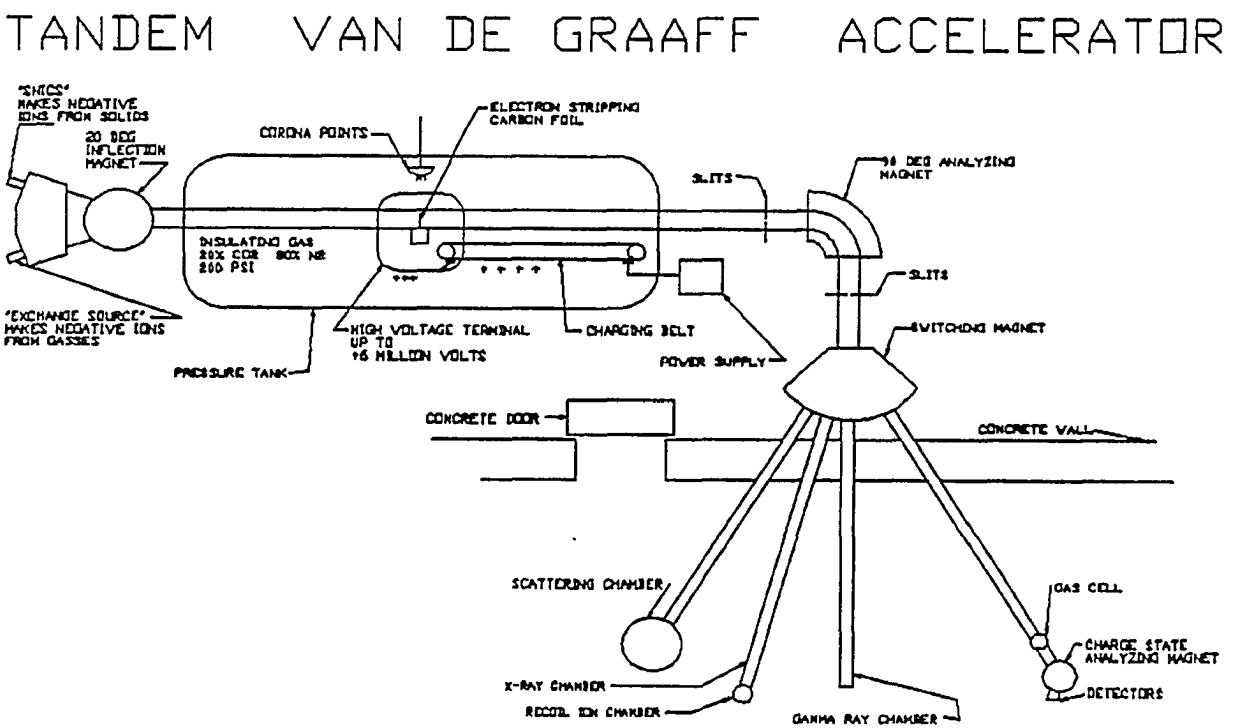

Figure 6. Schematic of the Tandem Van de Graaff Accelerator Facility at WMU.

desired energy were then selected with a 90° analyzing magnet. These ions were passed through a post-stripping foil to produce the desired S^{13+} ions, which were then selected with the switching magnet, and directed towards the atomic physics beam line.

A schematic of the experimental apparatus is shown in Figure 7. Two sets of collimating slits were designed to direct the incident projectiles into the target gas cell. After collimation, the S^{13+} ions entered the gas cell containing neutral target gases of He, Ne, or Ar. The geometrical length of the gas cell was 3.65 cm. The gas pressure was measured and adjusted by a capacitance manometer with a remotely-controlled valve. As the projectile beam passed through the target chamber, the interaction between the S^{13+} ions and the target gas atoms could lead to electron capture and loss and the formation of excited states. X-ray emission can then result from the decay of these excited states. A Si(Li) x-ray detector, which was mounted at 90° to the beam line, was used to detect emitted x rays and to measure their energy. For NTE, electron capture is associated with the formation of an intermediate excited state. Thus, in order to study NTE, it is necessary to isolate and select charge-changed projectile ions. The separation of the charge-changed and non-charge-changed components allows the measurement of the fraction

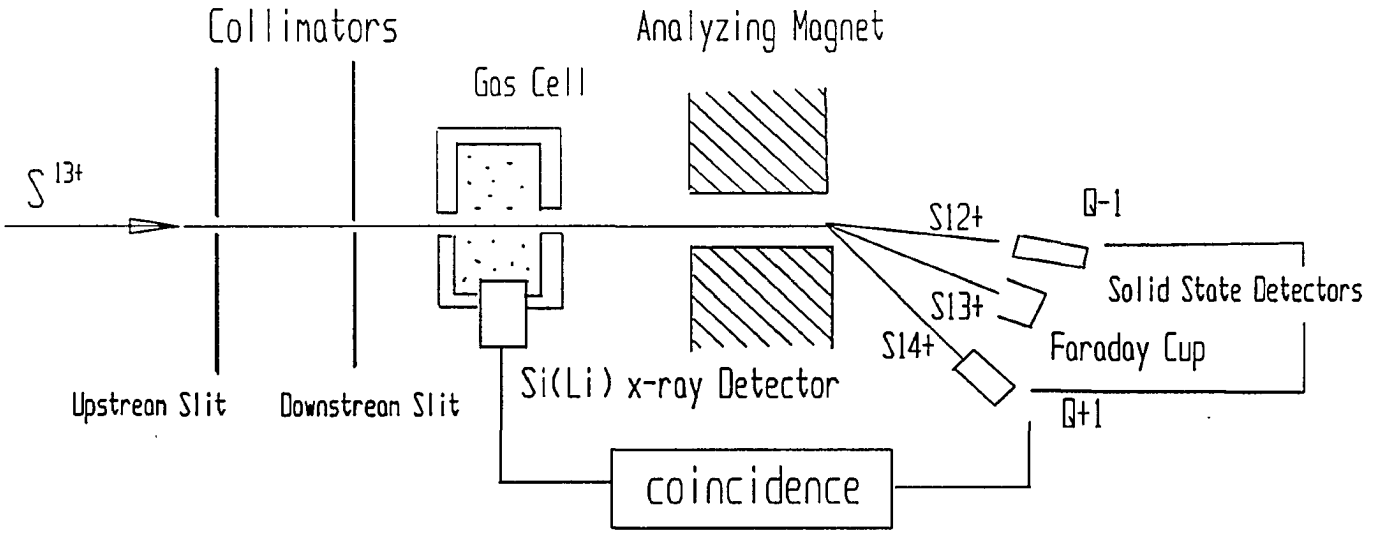

Figure 7. Schematic of the Experimental Apparatus for the Measurements Conducted Here.

fraction of projectiles which capture and lose electrons. Electron capture and the formation of an intermediate excited state leading to x-ray emission provide the signature for an NTE owing the interaction between the projectiles and the target gas atoms, the individual components of the charge-changed projectile beam were observed. The various outgoing charge-state components were separated by using an analyzing magnet as indicated in Figure 7. Solid-state surface-barrier detectors were used to observe charge-changed particle events which were subsequently counted with scalers. A Faraday cup was used to collect the main beam component, the current of which was measured with a Keithley electrometer.

A schematic of the electronics set-up used to carry out the measurements is shown in Figure 8. The incident particles strike the Faraday cup and produce a current which was measured with the electrometer which, in turn, gives an output of 0 to 2 volts proportional to the input current. This voltage output is connected to a 1 MΩ resistor thereby producing a current which is used as the input to a digital current integrator (DCI). The output of this integrator was "split" and subsequently input to both a LeCroy scaler and an ORTEC scaler, which were used to independently determine the total number of incident particles. The total number of incident particles not

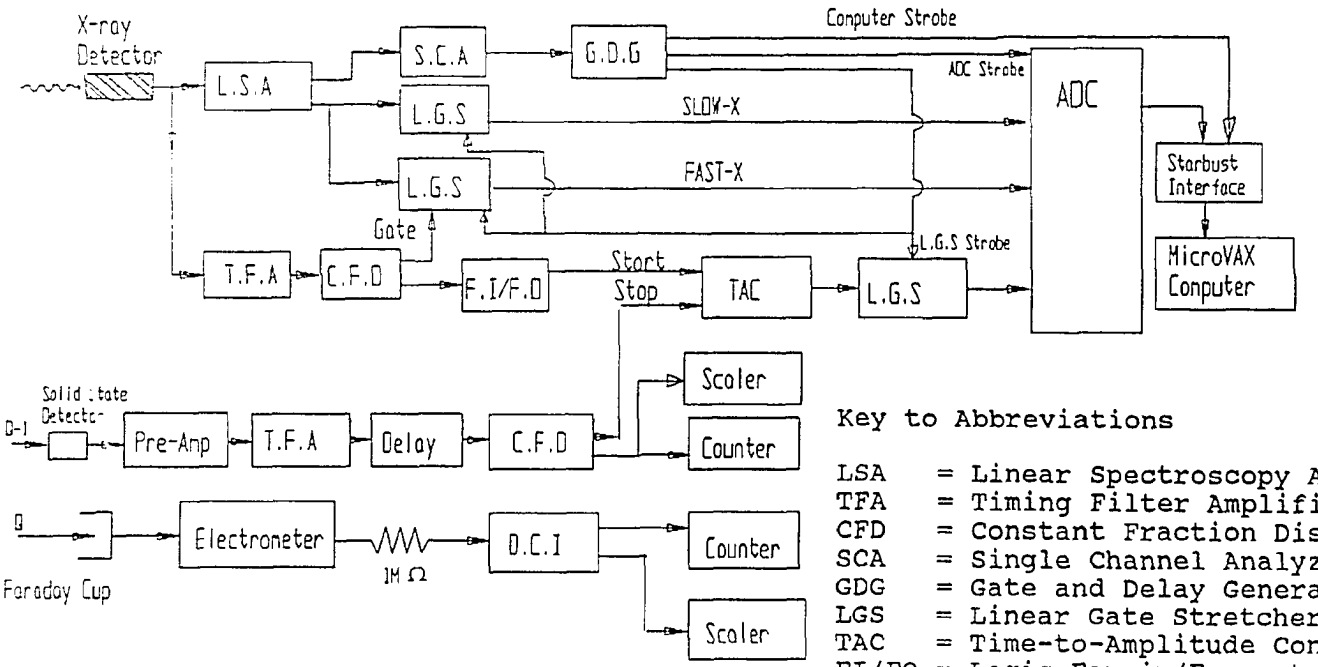

Key to Abbreviations

LSA = Linear Spectroscopy Amplifier
TFA = Timing Filter Amplifier
CFD = Constant Fraction Discriminator
SCA = Single Channel Analyzer
GDG = Gate and Delay Generator
LGS = Linear Gate Stretcher
TAC = Time-to-Amplitude Converter
FI/FO = Logic Fan in/Fan out
ADC = Analog/Digital Converter
DCI = Digital Current Integrator

Figure 8. Schematic of the Electronics Set-up.

involved in charge exchange was obtained by the integrating the Faraday cup current, using the DCI, over the time required to take the data.

In order to investigate NTE, the capacity to get information on coincidence events must be accomplished. The following basic pieces of data were collected and stored for each x ray detected: the energy of the x ray and, if a charge-changed projectile was detected, the time between x-ray detection and projectile detection. Valid coincident events all have the same relative timing. This time difference was measured using a time-to-amplitude-converter (TAC) which only outputs a signal if a START and a STOP signal are recorded within a pre-set time period.

The x-ray signal from the Si(Li) detector was split into two paths. One path, after passing through a linear spectroscopy amplifier (LSA), was used to produce an x-ray energy spectrum. The output signal from the LSA is routed through two parallel linear gate stretchers (LGS) which are used to stretch and hold these x-ray signals until a STROBE is provided by a gate and delay generator (GDG). The output signal from one LGS, labeled SLOW-X, is connected directly to the ADC. The LGS output labeled FAXT-X is gated by the logic signal used as the START signal for the TAC. Thus, the spectrum resulting from FAST-X corresponds to those x rays which give rise to this logic signal, while

the spectrum resulting from SLOW-X represents the total x-ray events detected. From the ratio of SLOW-X to FAST-X events, which is typically slightly greater than unity, a correction can be made for coincidence events which may be "lost" in the fast-timing logic signal electronics. The other signal from the Si(Li) detector was routed through a timing filter amplifier (TFA) and then input to a constant fraction discriminator (CFD) which converts the analog signal, whose amplitude is proportional to the energy of the x-ray pulse, into a logic signal if the amplitude is larger than the minimum setting on the discriminator. One output of the CFD was connected to a FAN IN/FAN OUT module which provides several identical output signals, while the other output was used as a logic gate to the FAST-X linear gate stretcher (LGS). One of the FAN IN/FAN OUT signals was used as a START signal for the TAC; other signal outputs were routed to various scalers and counters.

The output signals from the solid-state detectors were routed through pre-amplifiers and timing filter amplifiers (TFA). The signal from the TFA was delayed by about $1.3 \cdot 10^{-6}$ seconds to provide the necessary time difference between the START and STOP signals for the TAC. The delayed TFA output signals were then sent to a CFD. The logic signal from the CFD provided the STOP signal for the TAC. After receiving both a START and a STOP signal, the

TAC outputs an analog signal whose amplitude is proportional to the time difference between the START and STOP signals. The signal from TAC was then sent to a linear-gate-stretcher (LGS) which was used to stretch and hold the signal until the STROBE input was provided. The signals from the various LGS modules, after passing through an analog-to digital converter (ADC), were transmitted through a STARBURST interface module to a MicroVAX II computer system for sorting and storage.

For the NTE experiments, 20 - 70 Mev S^{13+} projectiles were used, and He, Ne and Ar were used as target gases. Data were taken for total single-electron capture and loss, total x-ray emission, and x-ray emission associated with single-electron capture (Q-1) and single-electron loss (Q+1). The gas pressure, measured with a capacitance manometer, was varied in the range from 0 to 100 mTorr. Each run was performed for a specific target gas-cell pressure. Three runs with different pressures were carried out at each projectile energy. The raw data obtained are the numbers of counts obtained from each of the particle detectors, the energy spectrum of x-ray events, and the time spectrum of coincidence events. The total number of incident particles for each run was determined from the current integration, while the total number of x-ray events and coincidence events were obtained from spectra

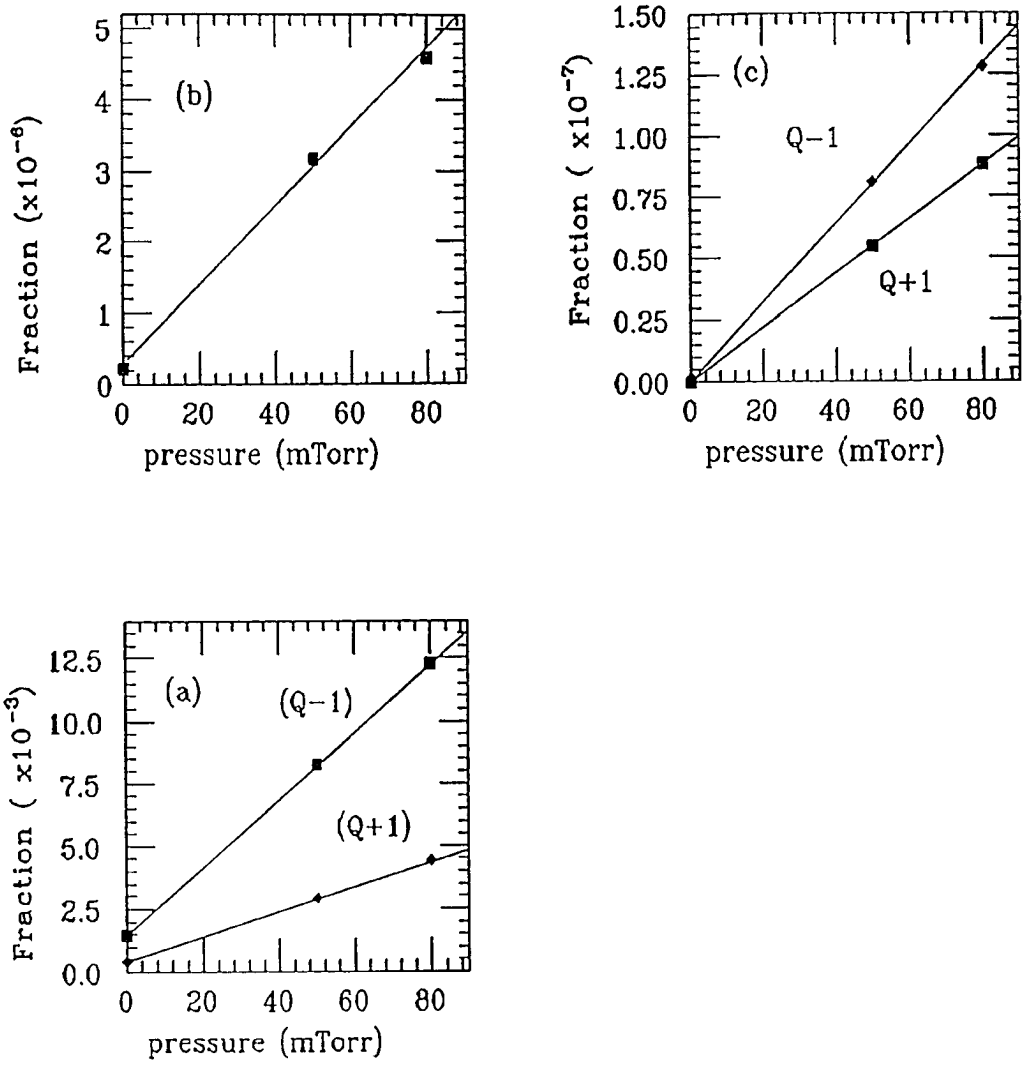

Figure 9. Typical Fractional Yields vs. Pressure for 60 MeV S^{13+} Projectiles Colliding With He. (a) Total Electron Capture (Q-1) and Loss (Q+1), (b) Total K x-ray Production, and (c) K X-Ray Emission Coincident With Electron Capture (Q-1) and Loss (Q+1).

which were recorded and sorted by the computer data acquisition system. In the range studied, linearity with pressure of the yields of particle events, x-ray events, and coincidence events was demonstrated, indicating that single-collision conditions were present (see Fig.9).

The calculation of cross sections and the discussion of experimental results is described in the following chapter.

CHAPTER IV

DATA ANALYSIS AND RESULTS

Determination of Cross Sections

NTE was investigated for 20 - 70 Mev S^{13+} projectiles incident on He, Ne and Ar targets. For each incident projectile energy, measurements were taken for three different gas-cell pressures. The spectra resulting from a run at a given pressure include the total x-ray events and x-ray events coincident with electron capture and loss. After correction for background and random coincidences, the spectra for each run were analyzed to obtain the fractional yields of the x rays of interest. The fractional yield is defined as the number of events of interest divided by the total number of incident particles. This yield was then plotted as a function of the gas-cell pressure, and a linear least-squares fit to the data was used to obtain the slope from which the cross sections could be calculated. The constants used to convert the slopes to cross sections are derived below. Single-electron capture and loss are observed with the particle detectors and x-ray events are observed with the Si(Li) detector, while the observation of coincidence events

depends on both detectors. Thus, the constants used to calculate the cross sections for single-electron capture and loss, and for x-ray events and coincidence events are different.

To calculate the cross sections, the total number of incident particles I_0 must be determined. Let N_{q-1},N_q, N_{q+1} be the numbers of projectile ions which undergo single-electron capture, no charge change, and single-electron loss, respectively. Then the total number of incident projectiles I_0 is given by :

$$I_0 = N_{q-1} + N_q + N_{q+1} \qquad (4.1)$$

where N_{q-1} and N_{q+1} were obtained directly from the number of events observed in the particle detectors, and N_q was calculated from the beam current integration (see Fig. 8). The incident beam was collected in a Faraday cup, and the current was measured with an electrometer. Assume that, in a time interval Δt, the number N_q particles strikes the Faraday cup. Then, the current produced can be expressed as follows:

$$I_q = \frac{N_q \times q \times 1.6 \times 10^{-19}}{\Delta t} \quad (C/s) \qquad (4.2)$$

Since this current I_q is measured by an electrometer with an output of 0 to 2 volts, with the 2 volt output occurring

when the electrometer reads full scale (typically 2 x 10^{-11} A), the output value V_q of the electrometer can be obtained from the following expression:

$$I_q : V_q = 2 \times 10^{-11} \text{ A} : 2 \text{ V}. \qquad (4.3)$$

Then

$$V_q = \frac{I_q \times 2}{2 \times 10^{-11}} \text{ (volts)}. \qquad (4.4)$$

Now, the voltage output V_q is dropped through a 1 MΩ resistor and the resulting current, which is equal to $V_q/10^6$ Ω, is measured by a current digitizer set to produce one pulse for every 10^{-8} Coulomb of input current. The total counts recorded from the current digitizer are related to the total charge input to the digitizer by the relation:

$$\frac{V_q}{10^6} \times \Delta t = \text{Scaler counts} \times 10^{-8} \text{ (C)} \qquad (4.5)$$

Then, from (4.2), (4,4) and (4.5), N_q can be expressed as:

$$N_q = 6.25 \times 10^{5} \times (\text{scaler counts/q}). \qquad (4.6)$$

Now, the fractional yield is defined as:

$$F = N / I_0 \qquad (4.7)$$

where N represents N_{q-1}, N_{q+1}, x-ray events N_x, or coincidence events N_{coin}.

The number of x-ray events N_x which were detected in the experiment is dependent upon the geometry of the target cell, the incident beam intensity I_0, the cross section for x-ray production σ_x, the x-ray detector efficiency ϵ_x, and the solid angle subtended by the detector $\Delta\Omega_x$. Specifically, the number of detected x-ray events is given by :

$$N_x = I_0 \sigma_x \epsilon_x (\Delta\Omega_x / 4\pi) T. \qquad (4.8)$$

The quantity $T = N_0 LP$ is the thickness of the target, where $N_0 = 3.3 \times 10^{13}$ at/cm^3·mTorr, L is the effective length of the target cell in cm, which must be corrected due to pressure variations near the entrance and exit apertures, and P is the pressure in mTorr in the target cell. Then, the fractional yield, F_x, of x rays detected, is given by:

$$F_x = N_x/I_0 = \sigma_x \epsilon_x (\Delta\Omega_x/4\pi)(N_0 LP). \qquad (4.9)$$

In Chapter III, it was shown that under single-collision conditions the fraction F_x depends linearly on the pressure P (see Fig. 9). Therefore

$$\Delta F_x/\Delta P = \sigma_x \epsilon_x (\Delta\Omega_x/4\pi)(N_0 L) \qquad (4.10)$$

and the cross section is given by :

$$\sigma_x = [\ 4\pi\ /\ (\epsilon_x\ \Delta\Omega_x\ N_0\ L)\ ]\ (\Delta F_x\ /\ \Delta P) \qquad (4.11)$$

where $\Delta F_x/\Delta P$ represents the slope of the fraction vs. pressure plot (see Fig. 9) which is determined directly from the linear least-squares fit. All cross sections of interest involving x-ray emission can be calculated from Eq. 4.11 if the length of the gas cell, the efficiency, and the solid angle subtended by the x-ray detector are known.

Similarly, in general, the relation between cross section and slope of the fraction vs. pressure curve can be expressed as:

$$\sigma = C\ (\Delta F\ /\Delta P) \qquad (4.12)$$

where the coefficient C varies depending on the particular detector which is used to detect the events of interest. In the NTE experiment, as discussed above, solid-state surface barrier detectors were used to detect electron capture and loss, and a Si(Li) detector was used to record x-ray emission. For total single-electron capture and loss, the surface barrier detectors detect all particles for each charge-state component. Thus

$$C = 1/(N_0\ L) \qquad (4.13)$$

and

$$\sigma = (1/N_0\ L)(\Delta F_x\ /\ \Delta P) \qquad (4.14)$$

is the expression used to calculate the total single-electron capture and loss cross sections.

Data Analysis

As discussed above, the raw data are the numbers of counts from each particle detector, the number of x-ray events, and the number of coincidence events. The number of total x-ray emission events and coincidence events were obtained from spectra such as those shown in Figure 10, in which channel number is related to x-ray energy. The spectra were sorted by the computer and recorded on tape. By appropriate gating, it was possible to distingush coincidence events associated with the projectile ion from those associated with the target atom. Fractional yields of the events of interest were plotted as a function of gas pressure and the slopes of these fraction vs. pressure plots were determined from linear-squares fits to the data. The ratio of SLOW-X to FAST-X slopes were used to correct the coincidence event slopes for "lost" events in the fast-timing logic signal electronics. From the geometry of the gas cell and Si(Li) detector, the x-ray energy, and the

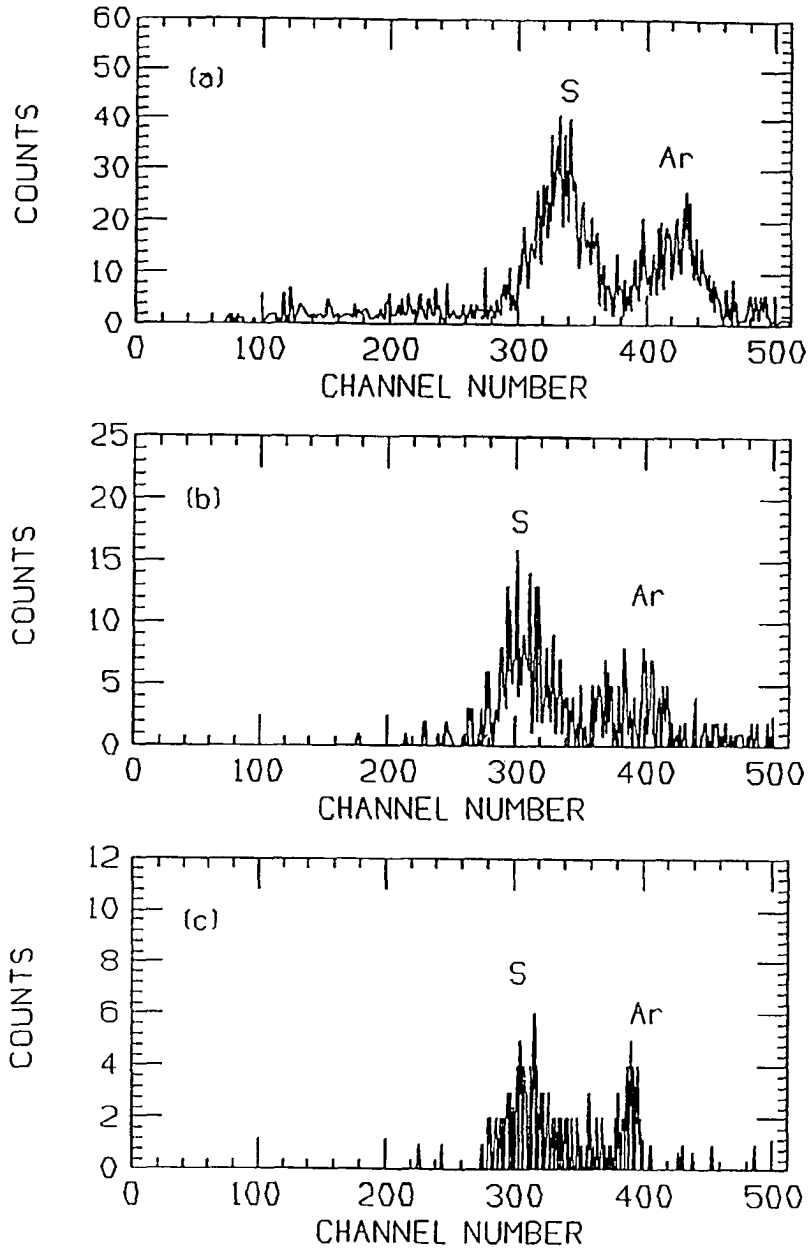

Figure 10. Typical X-ray Spectra for 60 MeV S^{13+} Projectiles Colliding With Ar at a Pressure of 10 mTorr.

(a) Total K X-Ray Production, (b) K X Rays Coincident with Electron Capture, and (c) K X Rays Coincident with Electron Loss.

detector solid angle and efficiency, the coefficients relating the slopes of the fraction vs. pressure curves to the cross sections (Eq. 4.11) were determined. Thus, the cross sections for the events of interest could be calculated. Errors in the cross sections were due mainly to statistical uncertainties in the least squares fits to the fractional yield vs. pressure curves. Considering other effects, the overall uncertainty in the measured cross sections is estimated to be less than ±20%.

Results

The measured cross sections obtained from the experimental data described in this thesis, along with the relative uncertainties, are listed in Tables 1 - 6 and shown in Figures 11- 13. Figure 11 shows all the measured cross sections as a function of the incident projectile energy for S^{13+} projectiles incident on He, including total single-electron capture and loss, total S^{13+} K x-ray emission, K x-ray emission coincident with electron capture, and K x-ray emission coincident with electron loss. Figure 12 presents the same cross sections for S^{13+} colliding with Ne, and, similarly, Figure 13 presents the cross sections for the Ar target. The contribution from NTE are contained in the σ_x^{q-1} cross sections listed in Tables 2, 4 and 6 and displayed in Figures 11, 12 and 13.

In the following Chapter, comparisons of the present results with previous studies, and a discussion of the present results, particularly those for NTE for the different targets, will be presented.

Table 1

Cross Sections for Total Single-Electron Capture and Loss, $\sigma_{q,q-1}$ and $\sigma_{q,q+1}$, Respectively, for S^{13+} Projectile Ions Colliding With He Target Atoms

E(MeV)	$\sigma_{q,q-1}$ ($\times 10^{-18}$ cm^2)	$\sigma_{q,q+1}$ ($\times 10^{-19}$ cm^2)
40	3.26 ± 0.82	3.94 ± 0.40
50	2.57 ± 0.26	4.01 ± 0.41
60	1.06 ± 0.12	3.78 ± 0.40

Table 2

Cross Sections for Total Projectile K X-ray Emission, σ_x, and for Single-Electron Capture and Loss Coincident With Projectile K x-ray Emission, σ_x^{q-1} and σ_x^{q+1}, Respectively, for S^{13+} Ions Colliding With He Target Atoms

E(MeV)	σ_x ($\times 10^{-20}$ cm^2)	σ_x^{q-1} ($\times 10^{-22}$ cm^2)	σ_x^{q+1} ($\times 10^{-22}$ cm^2)
30	0.78 ± 0.10	8.89 ± 0.90	3.36 ± 0.34
40	1.31 ± 0.13	7.86 ± 0.80	5.98 ± 0.60
50	1.64 ± 0.16	7.75 ± 0.78	8.18 ± 0.82
60	2.41 ± 0.24	3.35 ± 0.34	8.02 ± 0.80

Table 3

Cross Sections for Total Single-Electron Capture and Loss, $\sigma_{q,q-1}$ and $\sigma_{q,q+1}$, Respectively, for S^{13+} Projectile Ions Colliding With Ne Target Atoms

E(MeV)	$\sigma_{q,q-1}$ ($\times 10^{-17}$ cm^2)	$\sigma_{q,q+1}$ ($\times 10^{-18}$ cm^2)
30	5.56 ± 1.90	0.76 ± 0.20
40	4.51 ± 0.81	1.58 ± 0.16
50	3.10 ± 0.31	2.27 ± 0.23
60	1.98 ± 0.20	2.68 ± 0.37

Table 4

Cross Sections for Total Projectile K X-ray Emission, σ_x, and for Single-Electron Capture and Loss Coincident With Projectile K x-ray Emission, σ_x^{q-1} and σ_x^{q+1}, Respectively, for S^{13+} Ions Colliding With Ne Target Atoms

E(MeV)	σ_x ($\times 10^{-19}$ cm^2)	σ_x^{q-1} ($\times 10^{-20}$ cm^2)	σ_x^{q+1} ($\times 10^{-20}$ cm^2)
20	0.13 ± 0.02	0.35 ± 0.07	
30	0.61 ± 0.06	1.65 ± 0.20	0.15 ± 0.04
40	1.30 ± 0.16	3.99 ± 0.40	0.60 ± 0.10
50	1.64 ± 0.16	5.40 ± 0.54	1.54 ± 0.16
60	2.01 ± 0.50	4.80 ± 0.86	2.40 ± 0.24
70	1.45 ± 0.15	2.04 ± 1.16	4.40 ± 1.94

Table 5

Cross Sections for Total Single-Electron Capture and Loss, $\sigma_{q,q-1}$ and $\sigma_{q,q+1}$, Respectively, for S^{13+} Projectile Ions Colliding With Ar Target Atoms

E(MeV)	$\sigma_{q,q-1}$ ($\times 10^{-17}$ cm^2)	$\sigma_{q,q+1}$ ($\times 10^{-18}$ cm^2)
30	4.92 ± 0.49	0.41 ± 0.05
40	4.32 ± 0.43	0.91 ± 0.10
50	4.84 ± 0.45	1.51 ± 0.15
60	3.86 ± 0.39	2.27 ± 0.23
65	3.25 ± 0.33	2.50 ± 0.25

Table 6

Cross Sections for Total Projectile K X-ray Emission, σ_x, and for Single-Electron Capture and Loss Coincident With Projectile K x-ray Emission, σ_x^{q-1} and σ_x^{q+1}, Respectively, for S^{13+} Ions Colliding With Ar Target Atoms

E(MeV)	σ_x ($\times 10^{-19}$ cm^2)	σ_x^{q-1} ($\times 10^{-20}$ cm^2)	σ_x^{q+1} ($\times 10^{-20}$ cm^2)
20	1.12 ± 0.12	0.97 ± 0.10	
30	1.13 ± 0.11	1.78 ± 0.20	0.06 ± 0.01
40	1.19 ± 0.12	3.06 ± 0.31	0.15 ± 0.03
50	1.54 ± 0.16	4.67 ± 0.47	0.48 ± 0.05
60	2.01 ± 0.40	6.39 ± 0.64	1.46 ± 0.15
65	2.10 ± 0.21	6.05 ± 0.61	1.81 ± 0.18
70	1.45 ± 0.37	3.44 ± 0.34	4.35 ± 1.78

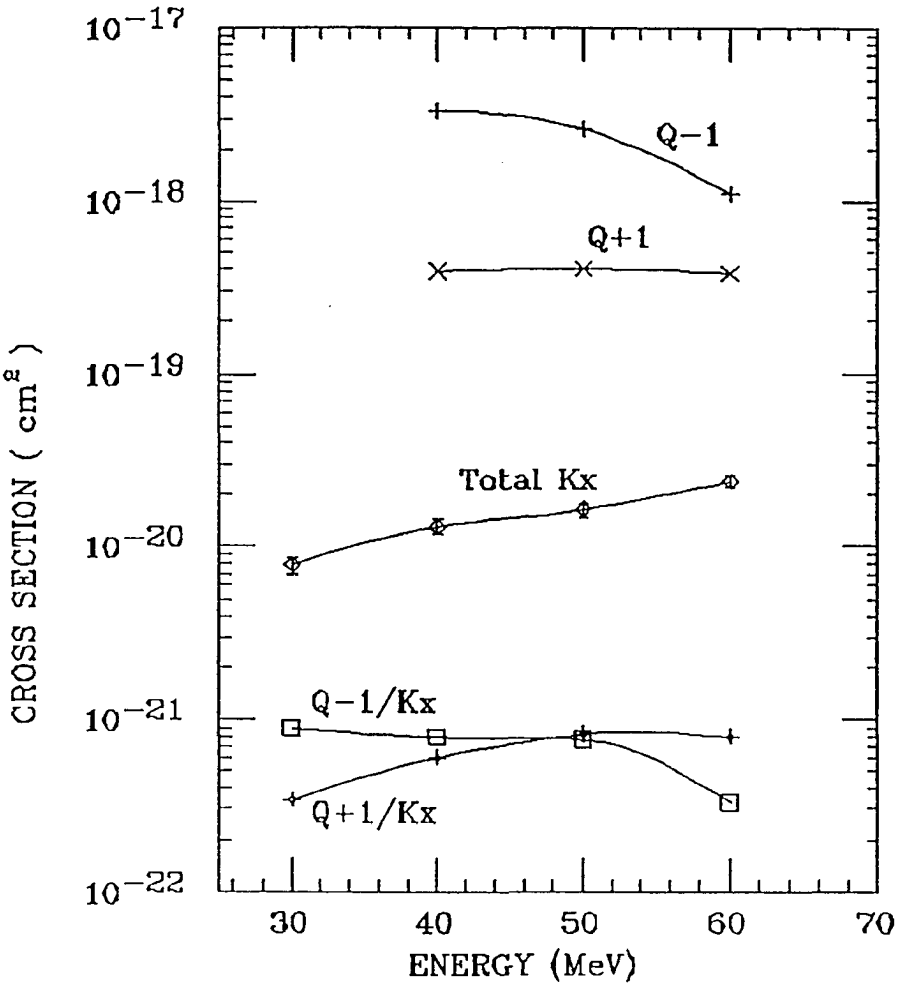

Figure 11. Measured Cross Sections for S^{13+} + He.

Total Projectile Single-Electron Capture (+) and Loss (×), Total Projectile K X-ray Emission (◇), and Projectile K X-ray Emission Coincident with Electron Capture (□) and Electron Loss (⊕).

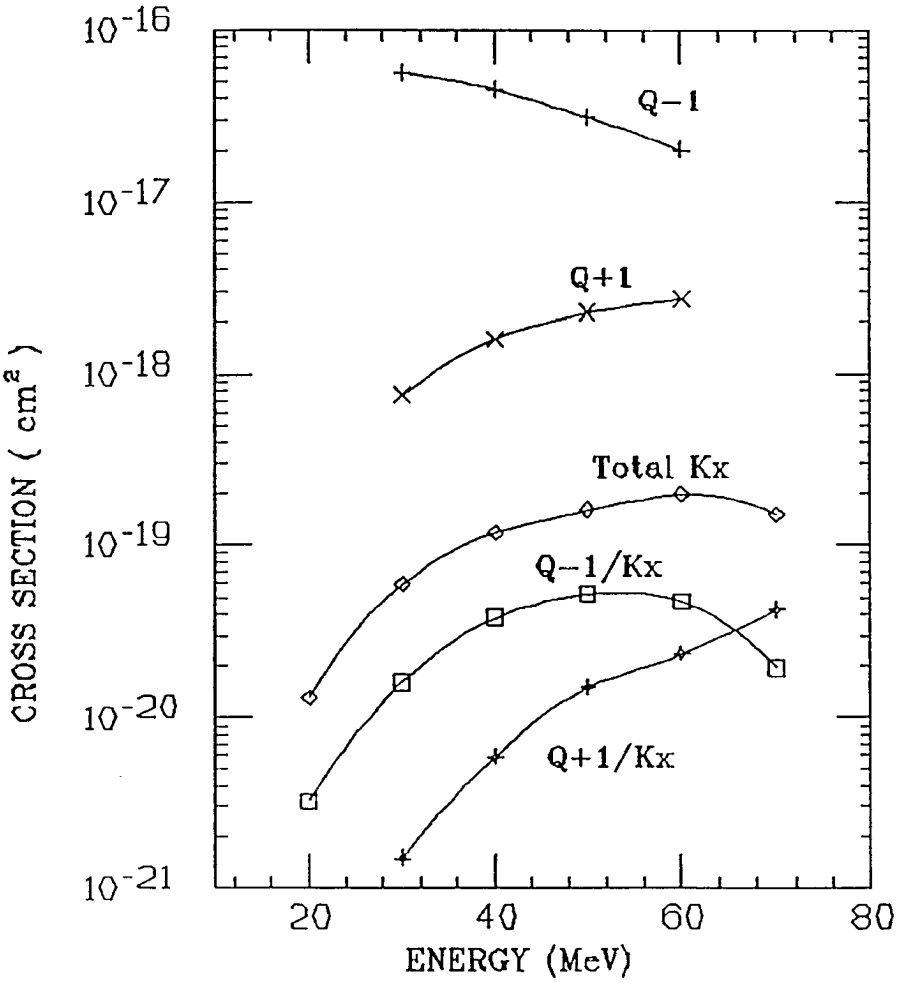

Figure 12. Measured Cross Sections for S^{13+} + Ne.

Total Projectile Single-Electron Capture (+) and Loss (×), Total Projectile K X-ray Emission (◇), and Projectile K X-ray Emission Coincident with Electron Capture (□) and Electron Loss (⊖).

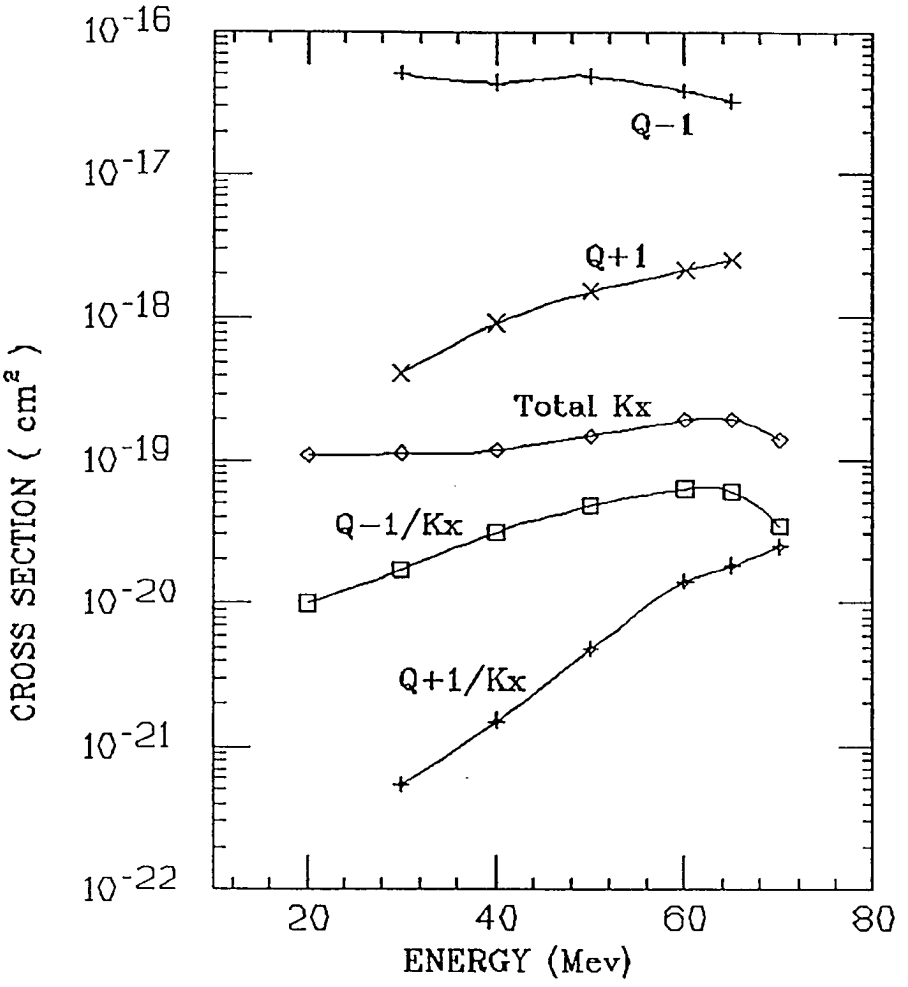

Figure 13. Measured Cross Sections for S^{13+} + Ar.

Total Projectile Single-Electron Capture (+) and Loss (×), Total Projectile K X-ray Emission (◇), and Projectile K X-ray Emission Coincident with Electron Capture (□) and Electron Loss (⊕).

CHAPTER V

DISCUSSION

K x Rays

The total K x-ray production cross sections versus projectile energy for S^{13+} incident on He, Ne and Ar, respectively, are given in Figure 14, along with previous data (Tanis et al., 1982, 1985, and 1992). The present results agree reasonably well with the previous data. The total x-ray production for the He target is much smaller than for the Ne or Ar target, since, for lower target atomic number Z, the Coulomb interaction between the target nucleus and the projectile electrons is weaker, thus resulting in a smaller probability for projectile excitation. Generally, as the target atomic number Z increases, the excitation probability is expected to increase. It is interesting to note, however, that while the total K x-ray production for Ar at the lowest projectile energies investigated is larger than that for the Ne target, at higher energies the total K x-ray production for Ne and Ar targets is almost the same.

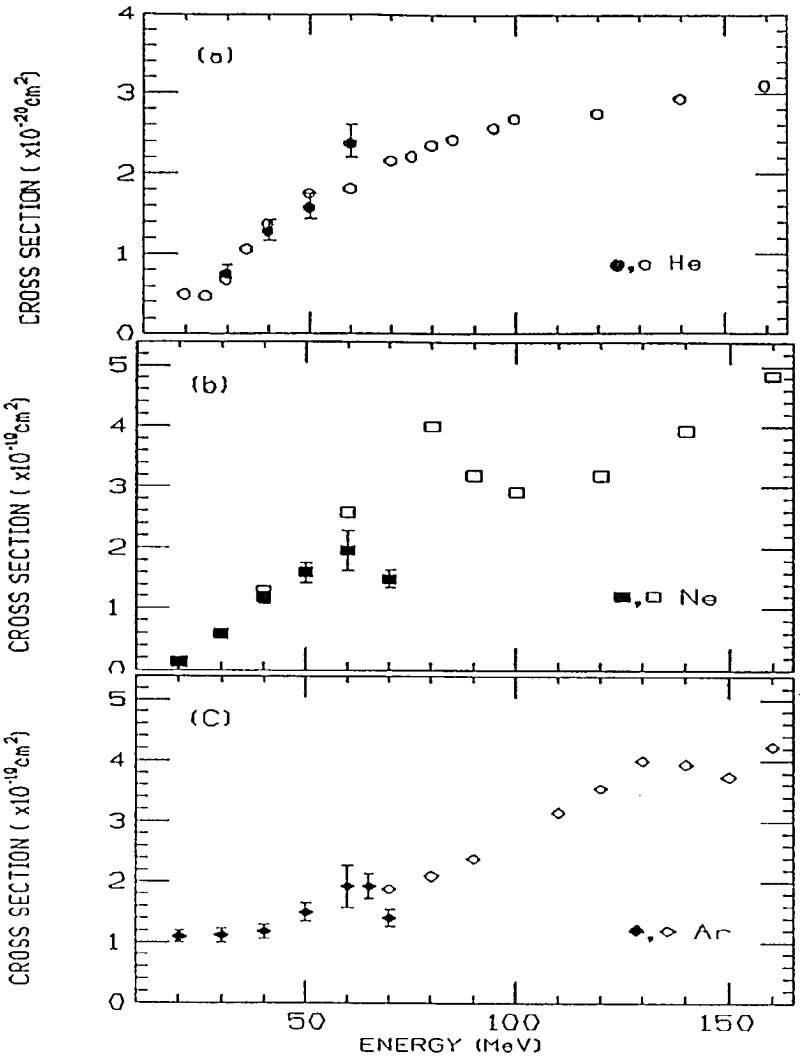

Figure 14. Cross Sections for Total Projectile K X-ray Production Versus Incident Projectile Energy for (a) S^{13+} + He, (b) S^{13+} + Ne, and (c) S^{13+} + Ar.

The solid symbols represent the present data, and the open symbols are the previous data of Tanis et al. (1982, 1985, and 1992).

K X Rays Associated With Electron Capture

The NTE data, represented by the cross sections for sulfur K x-ray emission coincident with electron capture for S^{13+} + He, Ne and Ar, are plotted in Figures 15, 16, and 17, respectively. Figure 18 displays the present and previous results, including both NTE and RTE cross sections. For S^{13+} + He, the previous data of Tanis et al. (1985) indicated that the NTE maximum for the He target occurs near a projectile energy of 30 MeV as shown in Fig. 19. For the Ne target (see Fig. 16), the cross section exhibits a broad peak with a maximum near 50 MeV, and from Figure 17 the NTE maximum for the Ar target is seen to occur near 60 MeV. Thus, these data display the dependence of the NTE cross section maximum on target atomic number Z.

From these data, it is seen that for targets with higher atomic number, the NTE maximum occurs at higher projectile energies and the maximum cross section becomes larger as shown in Figure 20. NTE is a two-step process, and the mechanisms involved are electron-nucleus interactions between the projectile nucleus and a target electron resulting in electron capture, and between the target nucleus and a projectile electron resulting in excitation. The dependence of the magnitude of the maximum NTE cross section on the atomic number Z of the target can be qualitatively explained in terms of the Coulomb excitation

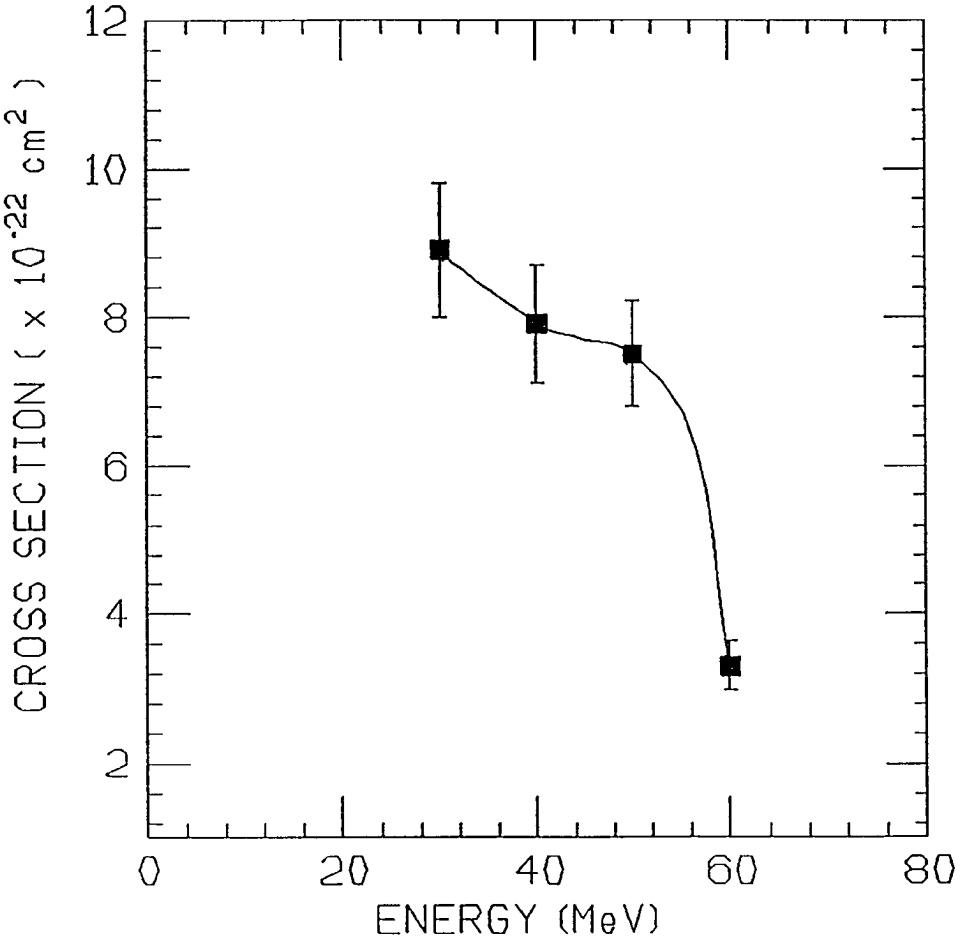

Figure 15. Measured Cross Sections for Projectile K X-ray Emission Coincident With Single-Electron Capture (NTE) for S^{13+} on He.

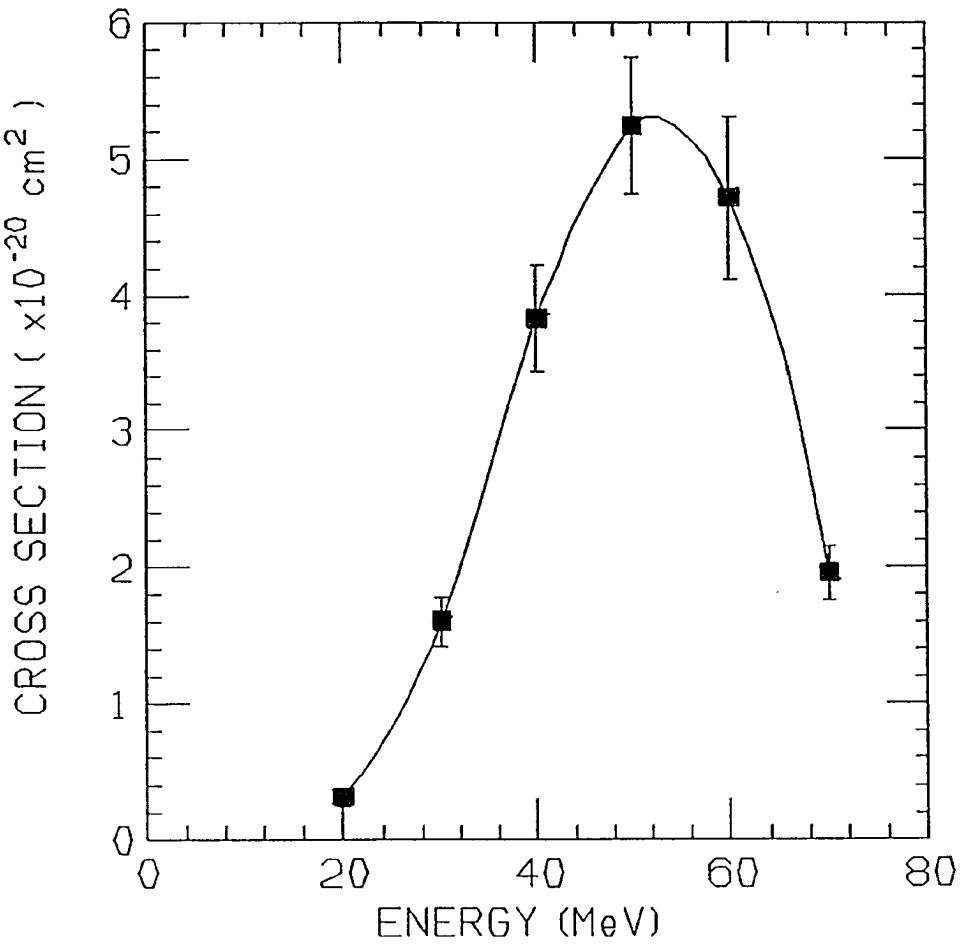

Figure 16. Measured Cross Sections for Projectile K X-ray Emission Coincident With Single-Electron Capture (NTE) for S^{13+} on Ne.

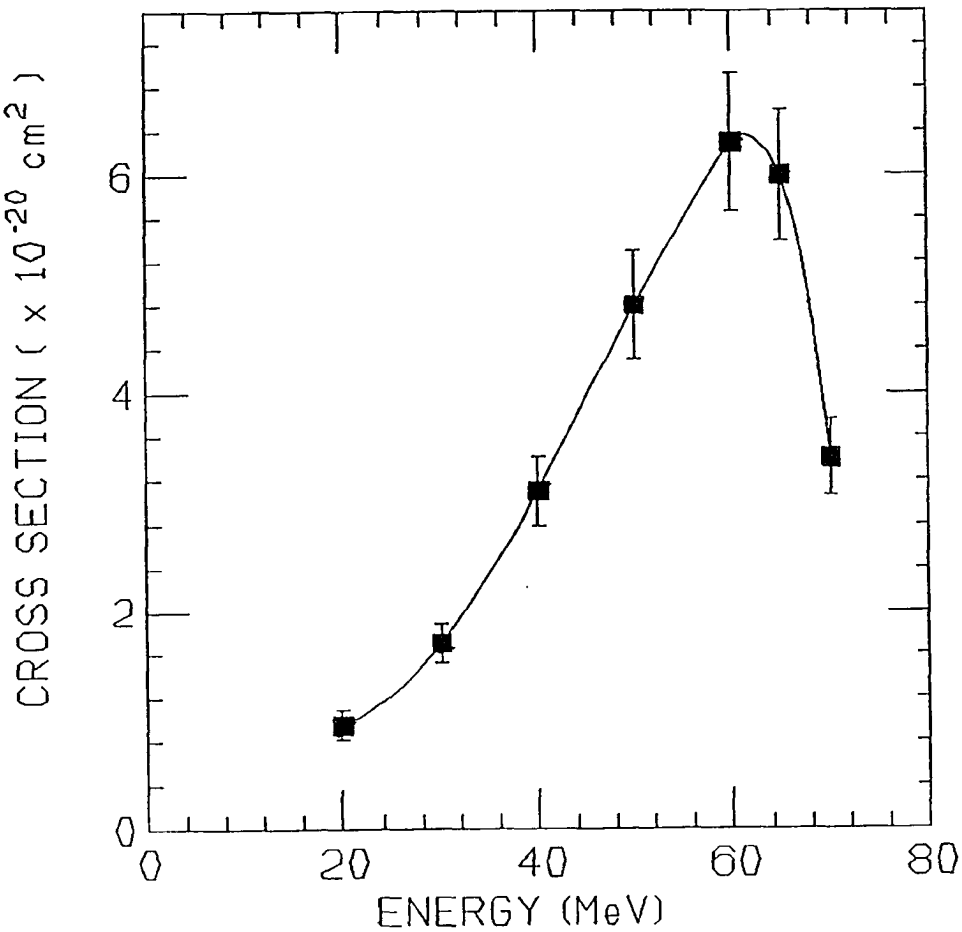

Figure 17. Measured Cross Sections for Projectile K X-ray Emission Coincident With Single-electron Capture (NTE) for S^{13+} on Ar.

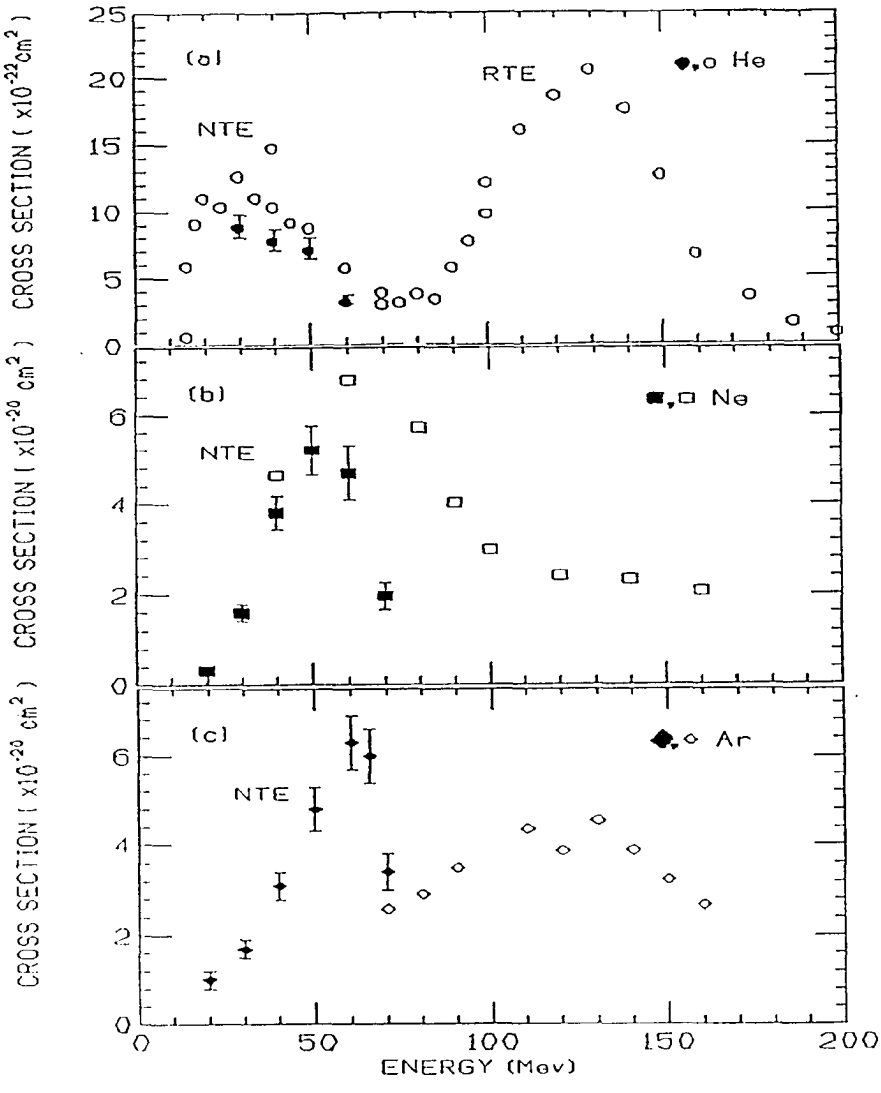

Figure 18. Cross Sections for Projectile K X-ray Emission Coincident With Single-Electron Capture (NTE and RTE) for S^{13+} Incident on (a) He, (b) Ne and (c) Ar.

The solid symbols represent the present data, and the open symbols are the previous data of Tanis et al. (1982, 1985, and 1986).

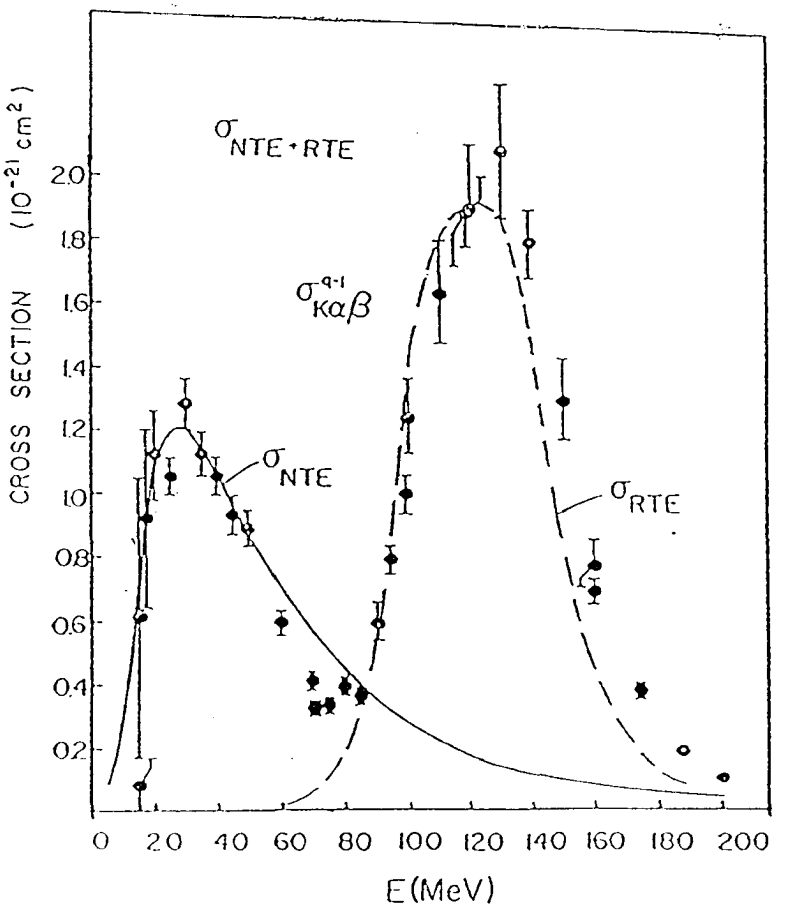

Figure 19. Cross Sections for K X-ray Emission Coincident With Single-Electron Capture in S^{13+} + He Collision from Tanis et al. (1985).

The maximum near 130 MeV is due to RTE and the maximum near 30 MeV is attributed to NTE. The dashed curve is the calculated RTE cross section multiplied by 0.85. The solid curve is the calculated NTE cross section normalized to the data.

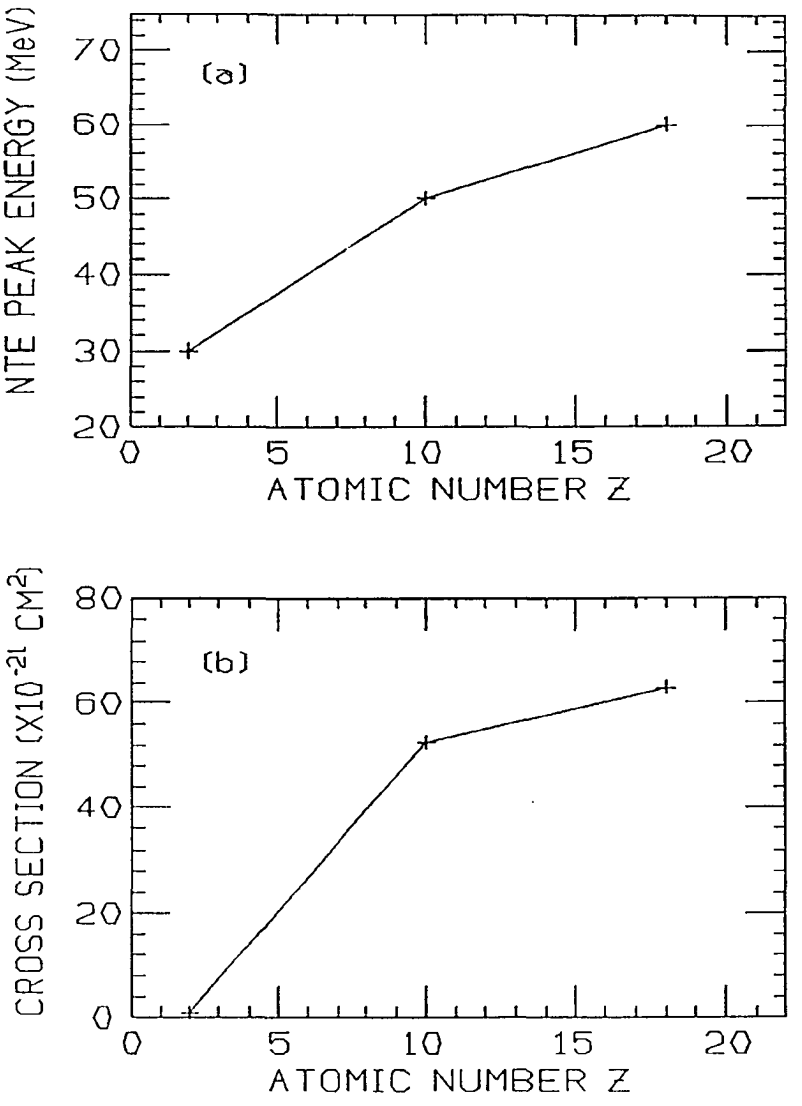

Figure 20. Dependence on Target Atomic Number Z of (a) the NTE Peak Position and (b) the Magnitude of the Maximum NTE Cross Section.

and capture probabilities for the different targets as follows. With higher target atomic number Z, the Coulomb interaction between the target nucleus and the projectile electrons becomes stronger, thereby increasing the probability for projectile excitation. Furthermore, since the number of electrons in the target is larger, the capture probability is increased. Qualitatively, the NTE maximum can be viewed as the result of the product of the total K-shell excitation cross section and the L-shell single-electron capture probablity at zero impact parameter as discussed in Chapter II. For the Ne and Ar targets, the total K x-ray production (mostly excitation) is nearly the same in the energy region of the NTE peak (40 - 70 MeV) (see Fig. 14), thus suggesting that the cross section for single-electron capture for small (≈ zero) impact parameter collision for the Ar target must be larger than that for Ne target in order for the NTE maximum cross section to be larger.

Figure 21 shows the cross sections for total single-electron capture versus projectile energy for S^{13+} incident on the three targets He, Ne, and Ar. Over the entire energy range investigated, the measured cross sections decrease with energy. At a given projectile energy, the target with higher atomic number has the larger capture cross section. This increase of the cross sections with

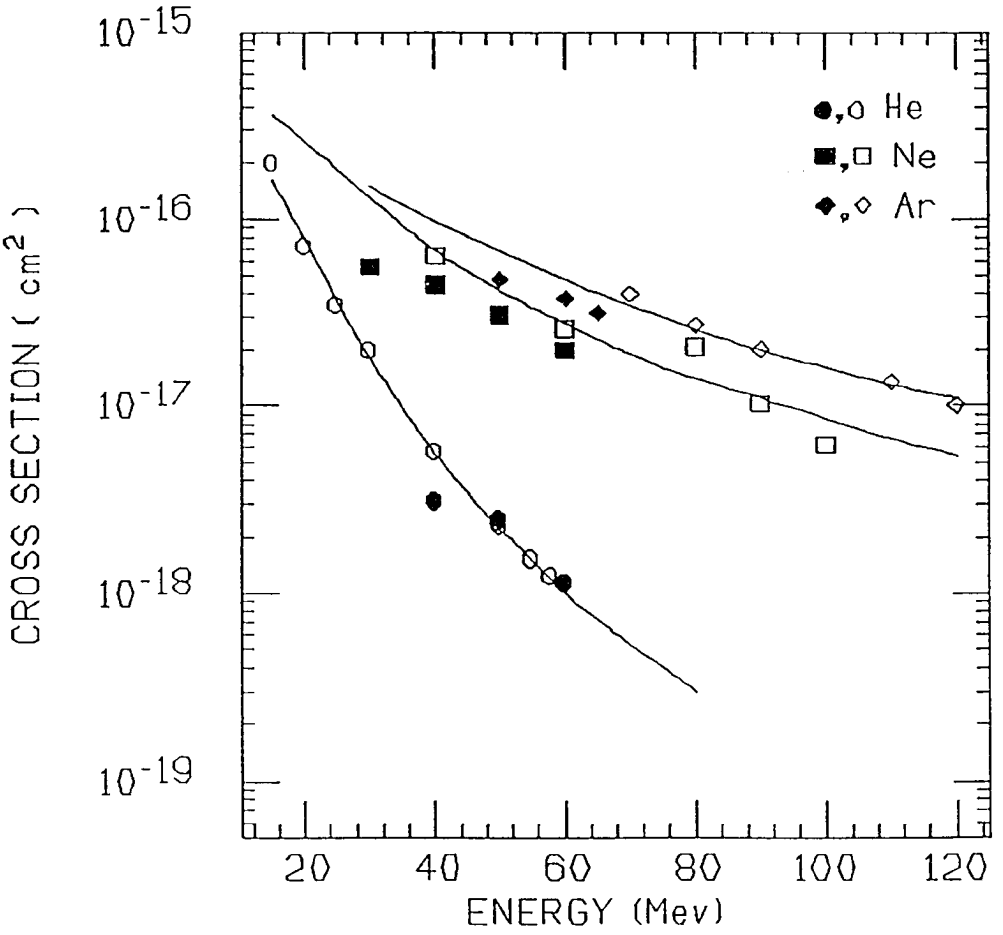

Figure 21. Cross Section for Total Single-Electron Capture for S^{13+} + He, Ne, and Ar.

The solid curves are the empirical scaling of Schlachter et al. (1983) and (1987). The solid symbols represent the present data, and the open symbols are the previous data of Tanis et al. (1982 and (1992) and Clark et al. (1986).

target atomic number is most likely due to the fact that targets with higher atomic numbers have more electrons, thus making the capture probability larger as expected from the discussed above. It is seen that the present and previous data are in generally good agreement with the empirical scaling of Schlachter et al., (1983 and 1987), however, some data differ by a factor of 2.

Now, as stated above, the maximum in the NTE cross section results from the product of the K-shell excitation cross section and the L-shell single-electron capture probability for small impact parameters. For targets with higher atomic numbers, the interaction between a projectile electron and the target nucleus gets stronger, resulting in a higher excitation cross section, and the availability of more electrons makes the capture probability larger. Thus, generally speaking, the NTE maximum for targets with higher atomic numbers is expected to have a larger cross section and to occur for higher projectile energies.

For the He target, both the excitation and capture cross sections are much smaller than those for the Ne and Ar targets, and, furthermore, for He the total single-capture cross sections decrease much more rapidly with increasing energy than those for Ne and Ar; thus, the NTE maximum for He occurs at a lower projectile energy with a smaller cross section. For the Ne and Ar targets, the

total K x-ray production (mostly due to excitation) is nearly the same in the region of the NTE maxmum (40 - 70 MeV). Thus, the difference in the magnitudes of the NTE cross sections for the Ne and Ar targets must come only from the difference in the capture cross sections at zero impact parameter, which results in a smaller difference between Ne and Ar compared with the difference between the He and Ne targets.

Based on the present results, the difference in the net Coulomb interaction between the target nucleus and the projectile electron, which results in projectile excitation, must increase relatively slowly between Ne (Z=10) and Ar (Z=20) in comparison with the increase from He target (Z=2). This suggests that the screening by the electrons in Ne and Ar is such that the resulting effective target charges giving rise to projectile excitation are almost the same for these two targets. This would explain why the total K x-ray production for the Ne and Ar targets is almost the same in the range of the NTE maximum, but much higher than that for the He target. Since the electron capture probability decreases less strongly with increasing energy as the target atomic number increases, the NTE maximum for Ne and Ar occurs for nearly the same incident projectile energies (50 and 60 MeV, respectively) compared with the He target for which the NTE maximum occurs for 30

MeV.

K X Rays Associated With Electron Loss

Finally, Figure 22 shows the cross sections as a function of projectile energy for projectile K x-ray emission coincident with single-electron loss for S^{13+} on He, Ne and Ar, respectively. The cross sections for the He target are smallest, and the cross sections for the Ne target are larger than those for the Ar target. Since the total K x-ray production (mostly excitation) for the Ne and Ar targets is nearly the same at projectile energies 40 - 70 MeV, the larger coincidence cross sections for the Ne target are caused by the larger values of the single-electron loss cross sections relative to those for the Ar target as shown in Figure 23. It is noted that the present results are generally in agreement with the previous results from Tanis et al., (1982 1986 and 1992).

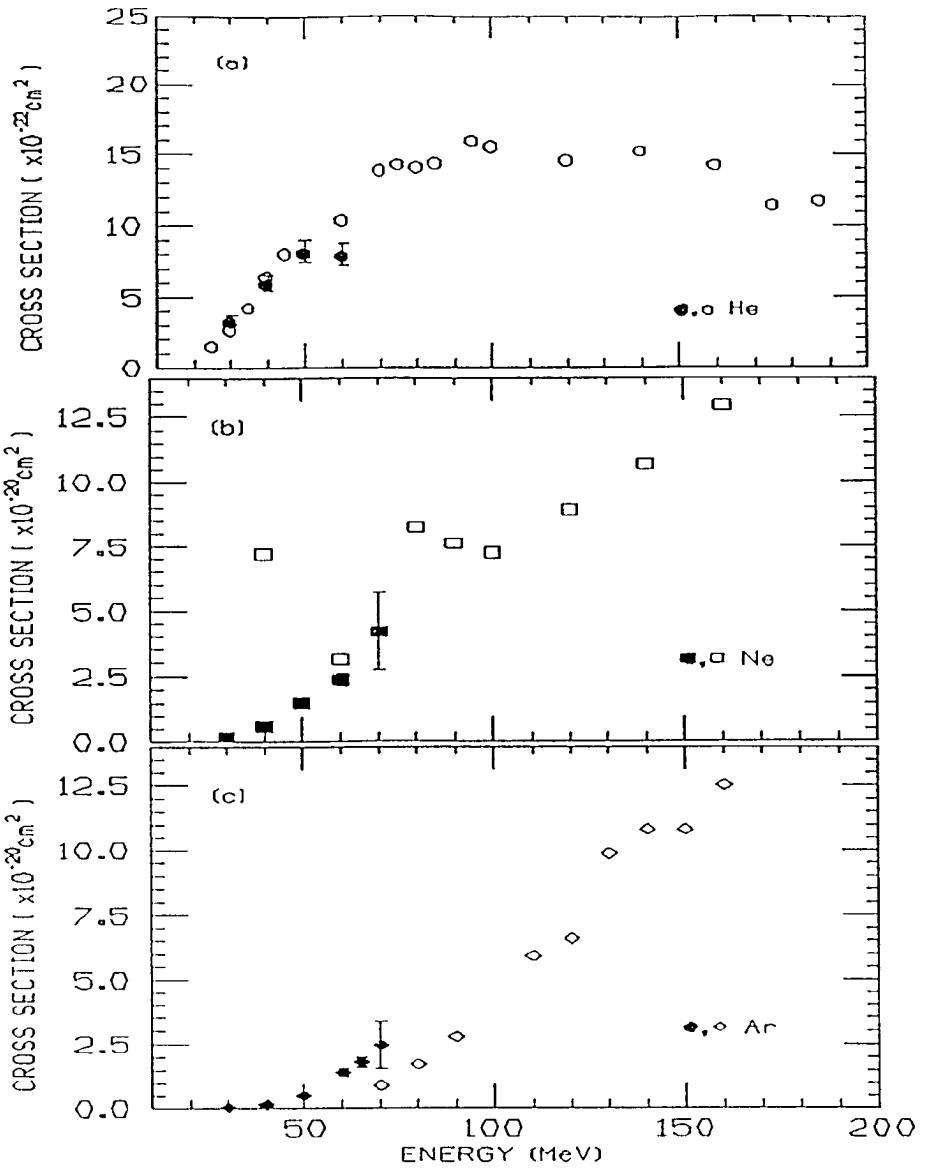

Figure 22. Cross Sections for Projectile K X-ray Emission Coincident With Single-Electron Loss for S^{13+} Incident on (a) He, (b) Ne, and (c) Ar.

The solid symbols represent the present data, and the open symbols are from the previous work of Tanis et al. (1982 and (1992).

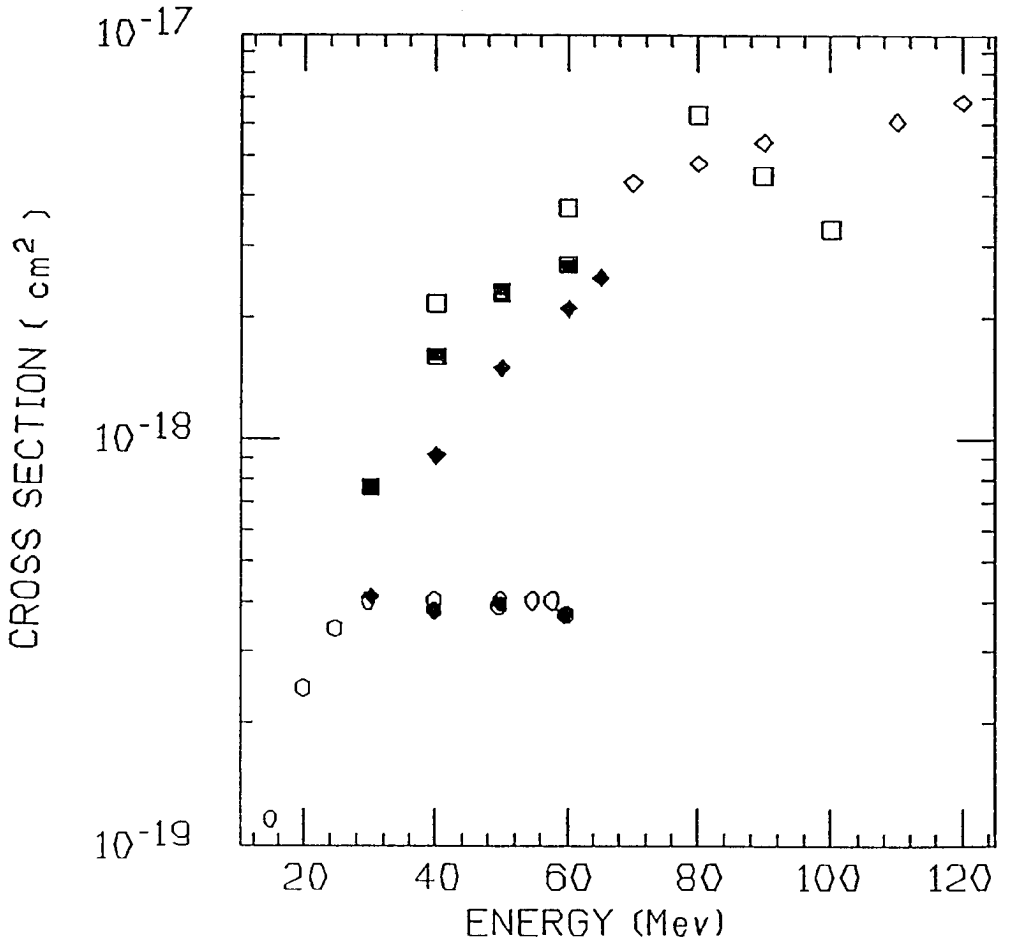

Figure 23. Cross Sections for Total Single-Electron Loss for S^{13+} + He, Ne, and Ar.

The solid symbols represent the present data, and the open symbols are the previous data of Tanis et al. (1986 and 1992).

CHAPTER VI

CONCLUSIONS

Non resonant transfer and excitation (NTE) has been investigated in the energy range from 20 - 70 MeV for S^{13+} projectiles incident on He, Ne and Ar, respectively, by detecting K x-ray emission in coincidence with single-electron capture. Additionally, cross sections were obtained for total single-electron capture and loss, total K x-ray production, and K x-ray production coincident with single-electron loss. All results were compared, where possible, with previous data and with theoretical predictions.

For total K x-ray production, the cross sections for Ne and Ar targets in the projectile energy range 40 - 70 MeV are nearly the same, and both are considerably larger than the corresponding cross sections for the He target. Since most of the total K x-ray production comes from projectile excitation, resulting from the Coulomb interaction between the target nucleus and the projectile electrons, the Ne (Z=10) and Ar (Z=18) targets with their higher atomic numbers have a stronger Coulomb interaction and thus are expected to have higher cross sections compared with the He target. The nearly identical total

K x-ray production cross sections for Ne and Ar targets at projectile energies 40 - 70 MeV indicates that screening of the nucleus by the electrons of these targets with their higher atomic numbers is significant, thereby resulting in a weaker than expected Coulomb interaction between the target nucleus and the projectile electrons. For single-electron capture, the target with higher atomic number shows larger cross sections, reflecting the availability of more electrons for capture.

The primary interest of this work was to investigate NTE for S^{13+} projectiles colliding with He, Ne and Ar targets. The NTE results show that for the He target with atomic number Z=2, the NTE maximum occurs at 30 MeV, while for Ne and Ar targets the NTE maxima occur at 50 and 60 MeV, respectively. Since NTE is a two-step process due to projectile K-shell excitation and electron capture to the L (or higher) shell, the NTE cross section is given approximately by the product of the K-shell excitation cross section and the single-electron capture probability at small impact parameters to the L-shell. For the Ne and Ar targets, which give rise to significantly higher total S^{13+} K x-ray production and single electron-capture cross sections compared with the He target, the NTE maximum cross sections and peak positions are also larger than those for the He target. Since the total S^{13+} K x-ray production

(mostly excitation) by Ne and Ar targets is nearly the same for projectile energies in the NTE region, the NTE cross section and peak position differences for these targets come mostly from differences in the total single-electron capture cross sections.

BIBLIOGRAPHY

Brandt, D. (1983a). Resonant transfer and excitation in ion-atom collisions. Physical Review, A27, 1314-1318.

Brandt, D.(1983b). A simple classical model for the impact parameter dependence of electron capture. Nuclear Instruments and Methods, 214, 93-96.

Hahn, Y., & LaGattuta, K.J. (1988) Dielectronic recombination and related resonance processes. Physics Reports, 166, 196-268.

Pepmiller, P.L. (1983). Formation of doubly excited two electron ions during F^{8+} + He, Ne or Ar collisions. Doctoral dissertation, Kansas State University, Manhattan, KS.

Pepmiller, P.L., Richard, P., Newcomb, J., Hall, J., & Dillingham, T.R. (1985). Formation of doubly excited two-electron ions during F^{8+} + He, F^{8+} + Ne, F^{8+} + Ar collisions. Physical Review, A20, 673 - 676.

Schlachter, A.S., Stearns, J.W., Berkner, K.H., Stockli, M.P., Graham, W.G., Bernstein, E.M., Clark, M.W., & Tanis, J.A. (1987). Electron capture for fast highly charged ions in He: An empirical scaling rule revisited. In Gedes, J., Gilbody, H.B., Kingston, A.E., Latimer, C.J., & Walters, H.J.R. (Eds.), Abstracts of Contributed Papers: Fifteenth International Conference of the Physics of Electronic and Atomic Collisions (p. 505). United Kingdom: Queen's University of Belfast.

Schlachter, A.S., Stearns, J.W., Graham, W.G., Berkner, K. H., Pyle, R.G., & Tanis, J.A. (1983). Electron capture for fast highly charged ions in gas targets: An empirical scaling rule. Physical Review , A27, 3372-3374.

Tanis, J.A. (1987). Electron transfer and projectile excitation in single collisions. Nuclear Instruments & Methods in Physics Research, A262, 52-61.

Tanis, J.A. (1990). Transfer excitation in ion-atom collisions. In Carlon, T.A., Kranse, M.O., & Manson, S.T. (Eds.), AIP Conference Proceedings, Fifteenth International Conference on X-ray and Inner-Shell Processes (pp. 359-374). New York: AIP.

Tanis, J.A. (1992). Private communication.

Tanis, J.A., Bernstein, E.M., Clark, M.W., Graham, W.G., McFarland, R.H., Morgan, T.J., Johnson, B.M., Jones, K.W., & Meron, M. (1985). Evidence for uncorrelated electron capture and K-shell excitation in S^{13+} + He collisions. Physical Review, A31, 4040-4042.

Tanis, J.A., Bernstein, E.M., Clark, M.W., Graham, W.G., McFarland, R.H., Morgan, T.J., Müller, A., Stockli, M.P., Berkner, K.H., Gohil, P., Schlachter, A.S., Stearns, J.W., Johnson, B.M., Jones, K.W., Meron, M., & Nason, J. (1986). Correlated electron capture and inner-shell excitation measurements in ion-atom collisions. In Lorents, D.C., Meyerhof, W.E. and Peterson, J.R. (Eds.), Electronic and Atomic Collisions (pp. 425-430). New York: Elsevier Science Publishing.

Tanis, J.A., Bernstein, E.M., Graham, W.G., Clark, M., Shafroth, S.M., Johnson, B.M., Jones, K.W., & Meron, M. (1982). Resonant behavior in the projectile x-ray yield associated with electron capture in S + Ar collisions. Physical Review Letters, 49, 1325-1328.